UNCLASSIFIED

AD NUMBER
AD460280
CLASSIFICATION CHANGES
TO: **UNCLASSIFIED**
FROM: **CONFIDENTIAL**
LIMITATION CHANGES
TO: **Approved for public release; distribution is unlimited.**
FROM: **Distribution authorized to U.S. Gov't. agencies and their contractors; Administrative/Operational Use; 14 FEB 1958. Other requests shall be referred to Air Force Research Labs., Hanscom AFB, MA.**
AUTHORITY
DNA ltr 25 Apr 1980 ; DNA ltr 25 Apr 1980

THIS PAGE IS UNCLASSIFIED

THIS REPORT HAS BEEN DELIMITED
AND CLEARED FOR PUBLIC RELEASE
UNDER DOD DIRECTIVE 5200.20 AND
NO RESTRICTIONS ARE IMPOSED UPON
ITS USE AND DISCLOSURE.

DISTRIBUTION STATEMENT A

APPROVED FOR PUBLIC RELEASE;
DISTRIBUTION UNLIMITED.

UNCLASSIFIED

~~CONFIDENTIAL~~

WT-1101

This document consists of 52 pages

No. [illegible] of 215 copies, Series A

1

AD No. 460280

DDC FILE COPY

Operation TEAPOT

NEVADA TEST SITE

February – May 1955

Official Classification of this report is
UNCLASSIFIED
although the original classification may not have been removed from all pages.
Classification changed by authority of TIS Change Notice No. ______
by ______ on ______

Project 1.1

MEASUREMENT OF FREE AIR ATOMIC BLAST PRESSURES

Issuance Date: February 14, 1958

UNCLASSIFIED

FORMERLY RESTRICTED DATA

Handle as Restricted Data in foreign dissemination. Section 144b, Atomic Energy Act 1954.

This material contains information affecting the national defense of the United States within the meaning of the espionage laws, Title 18, U.S.C., Secs. 793 and 794, the transmission or revelation of which in any manner to an unauthorized person is prohibited by law.

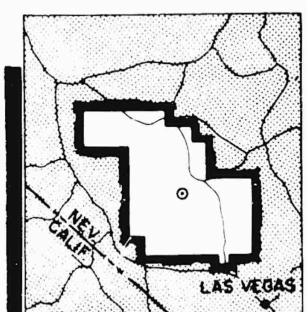

DDC
RECEIVED
APR 2 1965
DDC-IRA E

HEADQUARTERS FIELD COMMAND, ARMED FORCES SPECIAL WEAPONS PROJECT
SANDIA BASE, ALBUQUERQUE, NEW MEXICO

460280

~~CONFIDENTIAL~~

QUALIFIED REQUESTERS MAY OBTAIN COPIES OF THIS REPORT FROM DDC.
NOT FOR PUBLIC RELEASE.

Inquiries relative to this report may be made to

Chief, Armed Forces Special Weapons Project
Washington, D. C.

When no longer required, this document may be destroyed in accordance with applicable security regulations. When destroyed, notification should be made to

AEC Technical Information Service Extension
P. O. Box 401
Oak Ridge, Tenn.

DO NOT RETURN THIS DOCUMENT

QUALIFIED REQUESTERS MAY OBTAIN COPIES OF THIS REPORT FROM
NOT FOR PUBLIC RELEASE.

UNCLASSIFIED

~~CONFIDENTIAL~~

(18) AEC

(11) WT-1101

WT-1101

OPERATION TEAPOT—PROJECT 1.1

~~Report to the Test Director~~

(6) MEASUREMENT OF FREE AIR ATOMIC BLAST PRESSURES,

(10) by N. A. Haskell
James A. Fava, 2nd [redacted]
Richard M. Brubaker, [redacted]

Terrestrial Sciences Laboratory
Geophysics Research Directorate
Air Force Cambridge Research Center
Cambridge, Mass[redacted]

(11) 14 Feb 58,

(5) Air Force Cambridge Research Labs., Bedford, Mass.

UNCLASSIFIED

UNCLASSIFIED

~~CONFIDENTIAL~~

SUMMARY OF SHOT DATA, OPERATION TEAPOT

Shot	Code Name	Date	Time*	Area	Type	Latitude and Longitude of Zero Point
1	Wasp	18 February	1200	T-7-4†	762-ft Air	37° 05' 11.6856" 116° 01' 18.7366"
2	Moth	22 February	0545	T-3	300-ft Tower	37° 02' 52.2654" 116° 01' 15.6967"
3	Tesla	1 March	0530	T-9b	300-ft Tower	37° 07' 31.5737" 116° 02' 51.0077"
4	Turk	7 March	0520	T-2	500-ft Tower	37° 08' 18.4944" 116° 07' 03.1679"
5	Hornet	12 March	0520	T-3a	300-ft Tower	37° 02' 25.4043" 116° 01' 31.3674"
6	Bee	22 March	0505	T-7-1a	500-ft Tower	37° 05' 41.3860" 116° 01' 25.5474"
7	ESS	23 March	1230	T-10a	67-ft Underground	37° 10' 06.1263" 116° 02' 37.7010"
8	Apple	29 March	0455	T-4	500-ft Tower	37° 05' 43.9200" 116° 06' 09.9040"
9	Wasp'	29 March	1000	T-7-4‡	740-ft Air	37° 05' 11.6856" 115° 01' 18.7366"
10	HA	6 April	1000	T-5§	36,620-ft MSL Air	37° 01' 43.3642" 116° 03' 28.2624"
11	Post	9 April	0430	T-9c	300-ft Tower	37° 07' 19.6965" 116° 02' 03.6860"
12	MET	15 April	1115	FF	400-ft Tower	36° 47' 52.6887" 115° 55' 44.1086"
13	Apple 2	5 May	0510	T-1	500-ft Tower	36° 03' 11.1095" 116° 06' 09.4937"
14	Zucchini	15 May	0500	T-7-1a	500-ft Tower	37° 05' 41.3880" 116° 01' 25.5474"

* Approximate local time, PST prior to 24 April, PDT after 24 April.
† Actual zero point 36 feet north, 426 feet west of T-7-4.
‡ Actual zero point 94 feet north, 62 feet west of T-7-4.
§ Actual zero point 36 feet south, 397 feet west of T-5.

ABSTRACT

The purpose of Project 1.1 was twofold. First, it was designed to obtain peak free-air overpressure versus time measurements in the 10-to-2 psi range as a function of distance directly over a nuclear burst at a low scaled height. This information was to be used to establish the points in space at which the reflected and direct shock waves merge into a single shock wave and to determine the overpressure as a function of distance for the merged wave, in support of the Project 5.1 drone-aircraft lethal-volume studies. Second, it was desired to obtain free air peak overpressure versus distance measurements for an atomic burst at a high altitude.

To achieve the first objective, the project participated in two tower shots, Shot 4 and Shot 8, since their scaled heights approximated that of Shot 12 for which Project 5.1 required drone-aircraft positioning information. The operation was accomplished by deploying, from a B-29 aircraft, 10 parachute-borne instrumented canisters on each shot. The second objective was achieved by deploying 15 parachute-borne canisters from the strike aircraft on Shot 10.

On Shot 4, the canisters nearest the vertical above the shot were nearly 1,800 feet off, so that information directly applicable to Shot 12 was not obtained. However, the second shocks observed at these positions were extremely weak (11 to 13 percent of the strength of the direct shock) so that whether or not fusion of the two shocks takes place along the vertical, a large increase in peak overpressure above the free-air value is not anticipated.

In Shot 8, the canisters nearest the vertical were 1,600 to 2,100 feet off; in addition, the yield was far less than expected. As a result, no additional information applicable to drone-position planning for Shot 12 was obtained. However, Shots 4 and 8 produced useful data on the amplitude and arrival time of the reflected shock in the region of regular reflection, which will ultimately be required for complete specification of blast input to delivery aircraft.

On Shot 10, peak overpressure data were obtained over the range from 12.3 to 0.12 psi at approximate burst altitude (36,645 feet MSL). No significant change in effective blast energy at this altitude, compared to a low altitude burst, is indicated.

CONFIDENTIAL

FOREWORD

This report presents the final results of one of the 56 projects comprising the Military Effects Program of Operation Teapot, which included 14 test detonations at the Nevada Test Site in 1955.

For overall Teapot military-effects information, the reader is referred to the "Summary Report of the Technical Director, Military Effects Program," WT–1153, which includes the following: (1) a description of each detonation including yield, zero-point location and environment, type of device, ambient atmospheric conditions, etc.; (2) a discussion of project results; (3) a summary of the objectives and results of each project; (4) a listing of project reports for the Military Effects Program.

CONTENTS

FIGURES

TABLES

Chapter I
INTRODUCTION

1.1 OBJECTIVE

In the tower shots, the primary objective was to obtain peak overpressure data in the range of overpressures from 10-to-2 psi, i.e., slant ranges from 2,500 to approximately 7,000 feet. These data were needed in order to determine more accurately the point in space at which the incident and reflected shock waves directly above a nuclear burst merged into a single shock wave. In addition, there was a need to determine the overpressure as a function of distance in the merged shock wave, to determine the feasibility of positioning the drone aircraft of Project 5.1 for lethal-envelope studies. For this project a single (coalesced) shock wave was required---or an incident wave with a negligible following reflected shock---and it was necessary to determine the peak-overpressure-versus-distance relationship to permit the experimental aircraft to be properly positioned. These blast data may also have an ultimate application to the aircraft delivery problem.

Participation in Shot 10 was to record free air peak overpressure versus time as a function of distance for a nuclear burst at high altitude. The canister array was designed to obtain measurements in the overpressure range from 10-to-2 psi at approximate burst altitude. These data can be used ultimately for evaluating nuclear weapons for air-defense purposes.

1.2 BACKGROUND AND THEORY

<u>1.2.1 Shot 10.</u> The use of nuclear weapons in air defense will involve detonations at altitudes far greater than those used in previous tests. It is therefore necessary to determine whether current methods may be relied upon to predict properties of a high-altitude-shot blast wave from data obtained at much lower altitudes. In current practice a scaling law derived by R. G. Sachs (Reference 1) is used for this purpose. This law states that if f(R) is the peak-overpressure-versus-distance function for a 1-kt device fired at an

altitude h_1 where the ambient pressure is $P_o(h_1)$, then the peak overpressure at slant range R from a bomb of yield W fired at an altitude h_2, where the ambient pressure is $P_o(h_2)$, is given by:

$$\Delta P = k^3 f \left(\frac{kR}{S}\right)$$

$$k = \left[P_o(h_2)/P_o(h_1)\right]^{1/3} \qquad (1.1)$$

$$S = W^{1/3}$$

It is assumed that peak overpressure is to be measured as a function of distance along a horizontal line at the same altitude as the shot, so that the effect of a difference in ambient conditions between shot and gage need not be considered; however, for small yields and for overpressures within the range of interest, a simple correction for the difference in altitude between shot and gage may be obtained by substituting the gage altitude z for the shot altitude h_2 in the definition of the scale factor k. This is referred to here as modified Sachs scaling.

The Sachs scaling law for peak overpressure has been tested by the Ballistic Research Laboratories (BRL) by firing small high-explosive (HE) charges in a closed chamber under reduced atmospheric pressures corresponding to the ambient conditions at altitudes up to 50,000 feet (Reference 2). However, because of the great differences between the early stages of an HE and a nuclear explosion, the BRL results are not necessarily applicable. The case of a nuclear explosion at high altitude has been treated theoretically by F. H. Shelton (Reference 3) with the conclusion that there will be a reduction in effective blast yield with increasing altitude due to an increase in the loss of energy by early thermal radiation. His computations show a reduction in effective blast yield amounting to only 2 percent (relative to a sea-level burst) at 40,000 feet. Since a 2-percent reduction in yield reduces the range at which a given overpressure is reached by only 0.7 percent, far less than the accuracy with which an experimental overpressure-versus-distance curve can be established, Operation Teapot cannot be regarded as a definitive test of Shelton's theoretical computations.

In comparing the peak overpressures observed in Teapot with those predicted according to Equation 1.1, the basic overpressure-versus-distance function for a 1-kt device at a sea-level ambient pressure of 14.70 psi is that tabulated in Reference 6.

In addition to the peak overpressure, a knowledge of the blast pressure-time wave form is necessary for a complete analysis of blast effects on aircraft. A convenient parameter by which to express the wave form is the duration of the positive overpressure, scaled as follows. Let $\tau(R)$ be the free-air positive-phase duration as a function of range for a 1-kt device fired at an altitude where the ambient pressure is $P_o(h_1)$ and the ambient sound velocity is $c(h_1)$; then the positive-phase duration, T+ in seconds, for a device of yield W fired at an altitude h_2 is:

$$T+ \;=\; \frac{c(h_1)}{c(h_2)}\;\frac{S}{k}\;\tau\left(\frac{kR}{S}\right) \qquad (1.2)$$

1.2.2 Shots 4 and 8. For the purposes of Project 5.1, it was desired to position the drone aircraft on Shot 12 at points where they would be subjected to a single peaked shock. Photographic evidence from previous tests at low scaled heights of burst shows that, in addition to the merging of the direct and reflected shocks that begins at the ground surface and gives rise to the phenomenon known as Mach reflection, the reflected shock also overtakes the direct shock beginning at some point directly above the burst due to the abnormally high velocity of propagation of the reflected shock as it travels back through the intensely heated interior of the fire ball. Thus, at a certain stage there may be two single-peaked shocks, one rising from the ground and the other spreading laterally from a point above the shot. For scaled heights of burst below some minimum value, the two triple-point paths will presumably intersect, beyond which point the coalescence of the direct and reflected shock into a single shock will be complete. Since there were insufficient data on which to base a reliable prediction of the altitude above the shot at which the reflected shock would overtake the direct shock, it was desired that Air Force Cambridge Research Center (AFCRC) extend Project 1.1 to include pressure-time measurements in the 10-to-2 psi overpressure range directly above two tower shots before Shot 12, so that the information could be used to position the Project 5.1 drones to receive blast loads of the magnitude and character desired.

Shots 4 and 8 were chosen for this purpose with 10 pressure canisters allocated to each shot. Because of the probability of fairly large errors in positioning the canisters by parachute drop from the assigned aircraft altitude, it was decided to use a planned array consisting of a line of four canisters vertically above the shot, with offset vertical lines of three canisters each dropped 2,000 feet before and 2,000 feet after the central group.

Chapter 2
PROCEDURE

2.1 INSTRUMENTATION

For the three shots on which measurements were made, instrumented parachute-borne canisters were deployed from aircraft at a predetermined time so that the canisters would be at various slant ranges from the burst point at H-hour. Each canister was instrumented with two differential pressure inductance transducers (one having a scale ratio of approximately two with respect to the other), a pressure altimeter inductance transducer, and a radio telemetry transmitting unit. Each of the three transducers modulated the frequency of the sub-carrier oscillator to which it was connected. The outputs of the three sub-carriers were then mixed, and the output from the mixer frequency modulated the radio frequency carrier. This modulated RF was transmitted by a crystal-controlled transmitter whose power output was 1 1/2 to 2 watts. The modulated RF carrier for each canister was received at the ground recording station by an FM receiver tuned to the appropriate carrier. The output from each receiver was filtered so that the three sub-carrier frequencies were separated. Each sub-carrier was channeled to a discriminator which reproduced the original modulating signal. This signal---one which is electrically equivalent to the original variations of pressure---was fed to the galvanometers of the recording oscillographs.

For further details on the basic instrumentation, see Reference 4; however, the Multiple Object Tracking System (MOTS) canister equipment used in the earlier tests is no longer in use. The slant range was determined in the present test by photographic triangulation by Edgerton, Germeshausen, and Grier (EG+G).

In addition to the above basic pressure and telemetering instrumentation, each canister used on Shot 10 contained the Naval Research Laboratory (NRL) and Evans Signal Laboratory (ESL) equipment for Projects 2.2 and 2.1, respectively. This consisted of (1) fission detectors to determine the neutron flux and spectrum at altitude as a function of distance; (2) film badges to determine gamma-radiation initial dosage as a function of distance; and (3) a gamma-dose-rate device in three canisters only.

Three self-recording gages were included in Canisters 3, 7, and 8 on Shot 4. On Shot 8 three self-recording gages were also included in Canisters 1, 3, and 7. These gages were developed and fabricated by Shaw and Estes Inc. (Reference 5). Since they performed satisfactorily and their data compared favorably with the telemetered data, it is planned to develop a complete canister for utilizing this gage on future tests at the Nevada Test Site (NTS).

2.2 CALIBRATION

Reference is made to Operation Jangle report, Project 1.3c (Reference 4) for a description of normal field calibration procedure. In addition, post-test dynamic calibration of the pressure probe was carried out with the cooperation of BRL in the large BRL shock tube. The need for a dynamic calibration at high shock strengths became apparent when the canister-pressure measurements at short ranges on Shot 10 were compared with the peak overpressures obtained from the photographic measurements of shock velocity by Project 1.2 (Reference 7). The canister pressure measurements were definitely lower than those computed from the observed shock velocity, and since the overpressure-versus-time curves showed normal shock wave form, the applicability of the Rankine-Hugoniot equation relating shock velocity to peak overpressure could hardly be questioned. With the exception of Mike shot of Operation Ivy, previous measurements of blast pressures with parachute-borne canisters have been carried out at shock-pressure ratios (i.e., ratio of shock overpressure, ΔP_s, to ambient pressure, P_o) less than 0.27, while in Shot 10 this ratio was about 3.9 at the nearest canister from which data was obtained. At such high shock-pressure ratios the velocity of the flow behind the shock front is very high, and the perturbation of the flow caused by the presence of a pressure probe will in general result in an appreciable difference between the true free-field pressure and the pressure as measured by a gage connected to the probe. The correction factor for converting observed gage peak overpressures into free-field values should be a function of the angle of incidence of the shock front on the probe and of the Mach number of the flow behind the shock, which is a function of the shock pressure ratio. Details of the BRL shock-tube calibration tests are discussed in Appendix B. The results are presented in Figure 2.1 in a form suitable for direct determination of the peak overpressure correction factor from the observed gage readings. In this figure the ratio of free-field peak overpressure, ΔP_s, to gage peak overpressure, ΔP_g, is plotted as a function of the ratio of gage peak overpressure to ambient pressure, $\Delta P_g / P_o$, for angles of 0, 45, and 90 degrees between the axis of the pressure probe and the normal to the shock front. From a consideration of the scatter of the data on which these curves are based it is estimated that they are defined to a standard deviation of about 8 percent.

2.3 PARACHUTES

2.3.1 Shots 4 and 8. The system consisted of three parachutes: one 6-foot fist-ribbon parachute and two 28-foot square, semi-ribbon parachutes. The latter was designed at WADC for the specific purpose of minimizing oscillation of the canister during descent. As each canister was deployed from the aircraft, the 6-foot parachute was opened immediately by an attached static line. After a certain time interval, different for each canister and determined by the desired position of the particular canister in the array, a preset interval timer within the canister energized an ex-

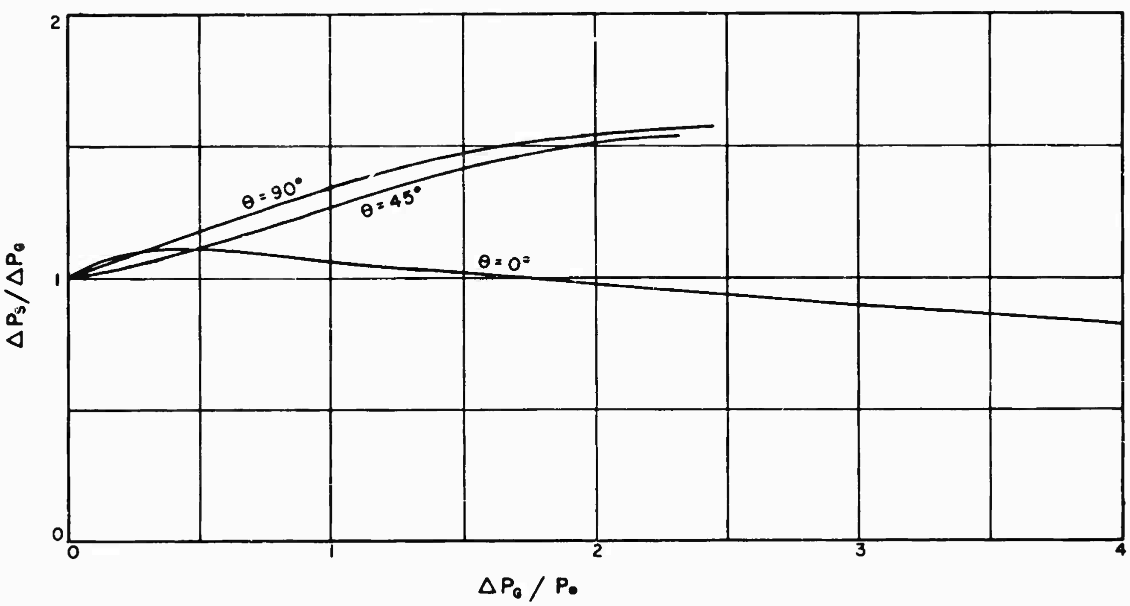

Figure 2.1 Pressure probe calibration curves.

plosive-squib line cutter which cut loose the 6-foot parachute. In both shots the interval timers were set to give the minimum practical time of fall on the 28-foot chute, consistent with the desired array position, in order to minimize the horizontal drift due to wind. A minimum of about 10 seconds on the 28-foot chute was allowed to reduce canister oscillation and permit the pressure within the reference chamber to reach ambient pressure before shock wave arrival. Since the first 28-foot chute was expected to burn off a number of canisters at H-hour, a second 28-foot chute together with a spring-loaded pilot chute were added.

In the event the first 28-foot parachute is destroyed by thermal radiation and the canister begins free fall, the pressure differential that develops across a pressure-actuated switch fires a squib cutter which deploys a second 28-foot chute. If thermal radiation does not destroy the first 28-foot chute, the pressure switch is closed by the blast wave after a pressure differential of 0.1 psi has been built up and the last chute is deployed at that point. To protect the last chute from thermal effects, the tail section of the canister was lengthened to make the overall length 91 inches.

The ballistics of both the 6-foot and 28-foot parachutes were known from previous tests.

2.3.2 Shot 10. The parachute system on this shot was also of a three-stage design: two 8-foot fist-ribbon parachutes and one 28-foot square, semi-ribbon parachute. The 8-foot chute was designed to give the canisters the same rate of descent as the weapon. The first 8-foot parachute was opened by a static line when the canister was deployed from the bomb bay of the strike aircraft. Each canister was allowed to remain on this parachute until the weapon was detonated. The second 8-foot parachute was deployed after the first one either had been destroyed by the thermal flux or had been released by the squib-cutting mechanism in the same manner as described for Shots 4 and 8. In order to facilitate recovery of the canisters, they were allowed to remain on the second 8-foot parachute until an altitude of approximately 18,000 to 20,000 feet MSL was reached. There, the second 8-foot parachute was released by the squib-cutting mechanism and the 28-foot parachute was deployed.

To determine the ballistics of the 8-foot parachute, dummy canisters were dropped from a B-36 aircraft at Edwards AFB, California. In the first practice drop, on 21 July 1954, the canister on an 8-foot parachute was approximately 825 feet horizontally and 350 feet vertically from the simulated weapon. This resulted in a slant range of approximately 900 feet, which was the distance at which the first canister was planned to be located based on a 3-kt yield. Six dummy canisters were deployed on a 12 October 1954 test drop, but all parachutes failed to open because static lines were not securely fastened to the aircraft.

On 12 January 1955, two completely instrumented canisters were test dropped to obtain ballistic information. The telemetering and parachute systems performed satisfactorily; however, no usable ballistics were obtained. A dummy canister was dropped on 9 March 1955, but ballistic information obtained was not received in time to be used on Shot 10. On the dry run for Shot 10, the first and fifteenth canisters of the proposed array were to be dropped. However, only the first canister was deployed, as a malfunction occurred in the intervalometer on the strike aircraft. The dropped canister was located by EG+G at zero time at 470 feet north, 180 feet below the burst---a slant range of approximately 528 feet.

2.4 AIRCRAFT POSITIONING

2.4.1 Shots 4 and 8. The determination of the correct initial drop point in space involved compensating for the integrated horizontal drift of the parachute-borne canisters due to the wind structure between the drop altitude and the altitude at which the shock wave arrived. The initial drop points were computed based on both the latest rawinsonde winds and the double drift winds obtained by the aircraft. Coordinates, e.g., 5,000 feet west and 2,000 feet north of ground zero, were relayed to the aircraft immediately prior to the actual drop.

In order to arrive over the drop point at a predetermined time, the aircraft flew a race-track pattern. This pattern, which had been worked out by the 6520th Flight Test Squadron on previous tests, consisted of two turns of exactly 2-minutes duration and two legs of approximately 4-minutes duration. Timing of the pattern starts when the aircraft initially passes over the drop point; the turns at both ends of the pattern have to be accurately timed and controlled at a uniform 90 degree per minute so that the midpoints can be taken as the reversal points of the turn. The time spent on the upwind and downwind legs depends upon the wind speed at drop altitude. To eliminate cross-drift, the pattern is oriented so that the final approach to the drop point is upwind.

2.4.2 Shot 10. Since the 15 canisters were deployed from the strike aircraft, the positioning of the aircraft with respect to the burst point was not a problem.

2.5 OPERATIONS

2.5.1 Shot 4. Ten parachute-borne instrumented canisters were deployed in clusters of three, four, and three from B-29 No. 4035 at an altitude of 22,920 feet MSL. A second B-29 aircraft, No. 1863, also loaded with 10 identically instrumented canisters, flew close formation with the drop aircraft. If the primary aircraft were not able to complete its mission, the alternate aircraft would have made the drop. The aircraft departed Kirtland Air Force Base and arrived over the Nevada Test Site at 0320 hours PST. Prior to the actual drop, the aircraft flew seven practice runs. Flight patterns were tracked and plotted on an MSQ-1 plotting board, and guidance data, with reference to time and position, were transmitted to the aircraft commander. The true inbound heading to the target on the first practice run was approximately 310 degrees. On each succeeding run the inbound heading shifted 5 to 10 degrees clockwise and the heading on the final run was 010 degrees. At H-125 seconds the first cluster of three canisters was deployed. The second and third clusters were released at H-122.6 and H-116.5 seconds, respectively. The position of the canisters at shock arrival time is shown in Figure 3.3.

The initial canister release point was determined to be 800 feet west and 1,068 feet south of ground zero, based on wind information obtained at H-3 hours. No canisters were directly over ground zero at shock-arrival time, due to wind shifts after the drop point had been determined, plus the fact that the aircraft arrived 12 seconds early at the drop point.

Of the 10 canisters dropped, usable information was obtained from eight. No peak-overpressure and arrival-time information was received from the canisters in array positions numbers 3 and 6. Number 3 was the high canister in the first vertical line and number 6 was the next to the highest canister in the vertical line of four canisters. The RF signal was lost on the two canisters at H-12 and H-8 seconds, respectively. Since the parachute system failed to operate properly, apparently due to power failure, they remained on the 6-foot parachute and struck the ground at the above mentioned times.

2.5.2 Shot 8. Ten parachute-borne instrumented canisters were deployed in clusters of three, four, and three from B-29 aircraft No. 4035 at an altitude of 24,780 feet MSL. The aircraft departed Kirtland AFB and arrived over the NTS at H-2 hour. Prior to the actual drop, the aircraft flew seven practice patterns. The flight patterns were tracked and plotted on an MSQ-1 radar plotting board and guidance data with reference to time and position were transmitted to the aircraft commander. The final true inbound heading was upwind at 270 degrees, and at H-122.7 seconds the first cluster of three canisters was deployed. The second and third clusters were deployed at H-115.9 seconds and H-110 seconds, respectively. The positions of the canisters at shock arrival time are shown in Figure 3.6. The horizontal and vertical spacing of the canisters was obtained in the same manner as on Shot 4. The initial canister release point was determined to be 1,935 feet east of ground zero, using wind information obtained at H-3 hour. The second and third clusters were released at 2,000-foot intervals based on the radar track. No canisters were directly over ground zero at shock-arrival time, due to wind shifts after the drop point had been determined. The aircraft arrived at the initial drop point approximately 2 seconds late.

Of the 10 canisters dropped usable data were obtained from eight. No peak overpressure and arrival time information was received from the canisters in array positions numbers 3 and 4. Number 3 position was the high canister in the first cluster and number 4 position was the lowest canister in the second cluster. The RF signal was lost on canister number 3 at H-97.8 seconds, and no RF signal was received from canister number 4. Both failures were apparently due to power supply malfunction.

2.5.3 Shot 10. The parachute-borne instrumented canisters were deployed from the strike aircraft at predetermined intervals after bomb release. Originally, it was thought that a horizontal array could be obtained by snubbing each successive parachute. However, the snubbing would have decreased the effective area of the parachutes, thereby causing the vertical velocity of the canister to increase and changing the ballistics of the parachute. It was therefore decided not to snub the parachutes and accept an array in which the canisters were not at the same altitude as the weapon.

To obtain the desired slant ranges, both the length of the bomb bay and the vertical spacing of the individual shackles were taken into account. Since the ground speed of the aircraft was approximately 500 ft/sec, an error of 1 second in a canister leaving the bomb bay would have resulted in an error of 500 feet in the horizontal separation of the canisters. A high-speed electronic intervalometer on the B-36 was utilized to deploy the canisters. The range of the intervalometer is from 0.2 to 31.2 seconds, or 100 to 15,600 feet at 100-foot intervals. Since both the weapon and the canisters were dropped from the same aircraft and in this case the canisters after the weapon, a synchronizing pulse was utilized to start the intervalometer. This pulse occurred at the time the weapon was released. For this particular drop, the canisters were deployed at various intervals from 1.6 to 22.2 seconds after the weapon was released.

Usable data were obtained from 11 of the 15 canisters dropped. No peak overpressure measurements were obtained from the canisters in array position No. 1, 2, 3, and 12. The RF signal from canister No. 1 was lost at H-hour, recovered at H+2 seconds for 0.2 seconds, after which there was no signal until H+10.3 seconds. For the next 40 seconds there were intermittent signals lasting 0.1 second every 0.5 second. This indicates that all parachutes were destroyed by thermal radiation and the canister was tumbling in free fall. The RF signal from canister No. 2 was also lost at H-hour and did not come back on until H+1.92 seconds, so that no overpressure measurement was obtained. No RF signals were received from canisters No. 3 and 12, apparently because of power supply failure. The horizontal and vertical spacing of the canisters at shock-arrival time is shown in Table 3.6.

Chapter 3
RESULTS

3.1 SHOT 4

Canister coordinates with respect to ground zero at shock arrival time are given in Table 3.1. These have been obtained by applying a small correction for canister drift and fall during shock travel time to the coordinates at zero time, which were determined photographically by EG+G. The over-all accuracy is believed to be better than ±50 feet in all coordinates.

Tracings of the telemetered overpressure versus time curves are shown in Figure 3.1. Small second shock arrivals are clearly shown by the traces from canisters 2, 4, 5, and 7. The telemetered signal from canister No. 1 was lost during the interval from 1.850 to 1.898 seconds, due to oscillation of the canister, but extrapolation of the trace indicates that it is very probable that a second shock of about 1-psi pressure increment arrived during this interval. Canisters 8 and 9 show no second shock and were presumably in the region of Mach reflection. Because of its extremely small amplitude, it is questionable whether or not the second arrival at canister 10 is to be interpreted as the ground reflected wave. There is, however, some prior evidence (Reference 6) that the reflected shock does become much weaker in the immediate neighborhood of the triple point, and it is therefore tentatively assumed that this canister was very close to the path of the triple point.

Peak overpressure and time of arrival of the first and second shocks are tabulated in Table 3.2. In the case of the second shock, the peak overpressure is taken with reference to the pressure existing immediately prior to the arrival of this shock. The column headed ΔP_g is the peak overpressure of the direct shock as read from the telemetered gage records. The column headed ΔP_1 is the corrected peak overpressure of the direct shock obtained by multiplying ΔP_g by the calibration factor plotted in Figure 2.1. Since the actual angle of incidence of the shock front on the canister probe is unknown, it is necessary to compute this angle on the assumption that the canister is hanging vertically at shock arrival time. However, it is believed that the amplitude of canister oscillation prior

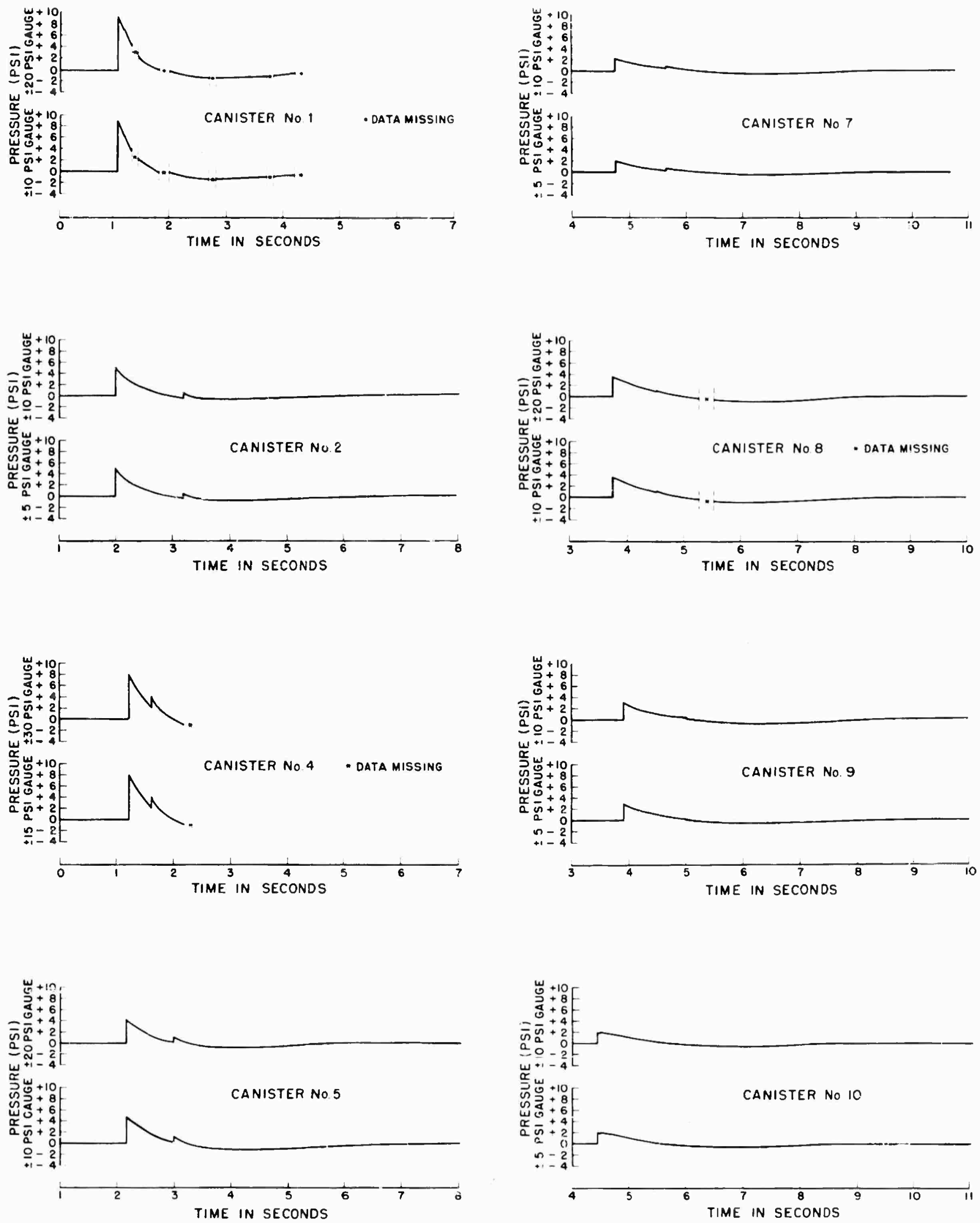

Figure 3.1 Shot 4 pressure versus time curves.

to shock arrival is small enough so that the error introduced by this assumption is far less than the uncertainty in the calibration curves themselves.

Peak overpressure of the first shock reduced to standard sea level conditions is plotted against reduced slant range in Figure 3.2. The so-called modified Sachs scaling has been used in the reduction to sea level. The reduced peak overpressure is defined as $\Delta P_1/k^3$, where $k^3 = P_o(z)/P_o(o)$ and the reduced slant range is kR. In the definition of k^3, $P_o(z)$ is the ambient pressure at the canister altitude, as determined from the photographic coordinates and the meteorological data, and $P_o(o)$ is the standard sea level atmospheric pressure,

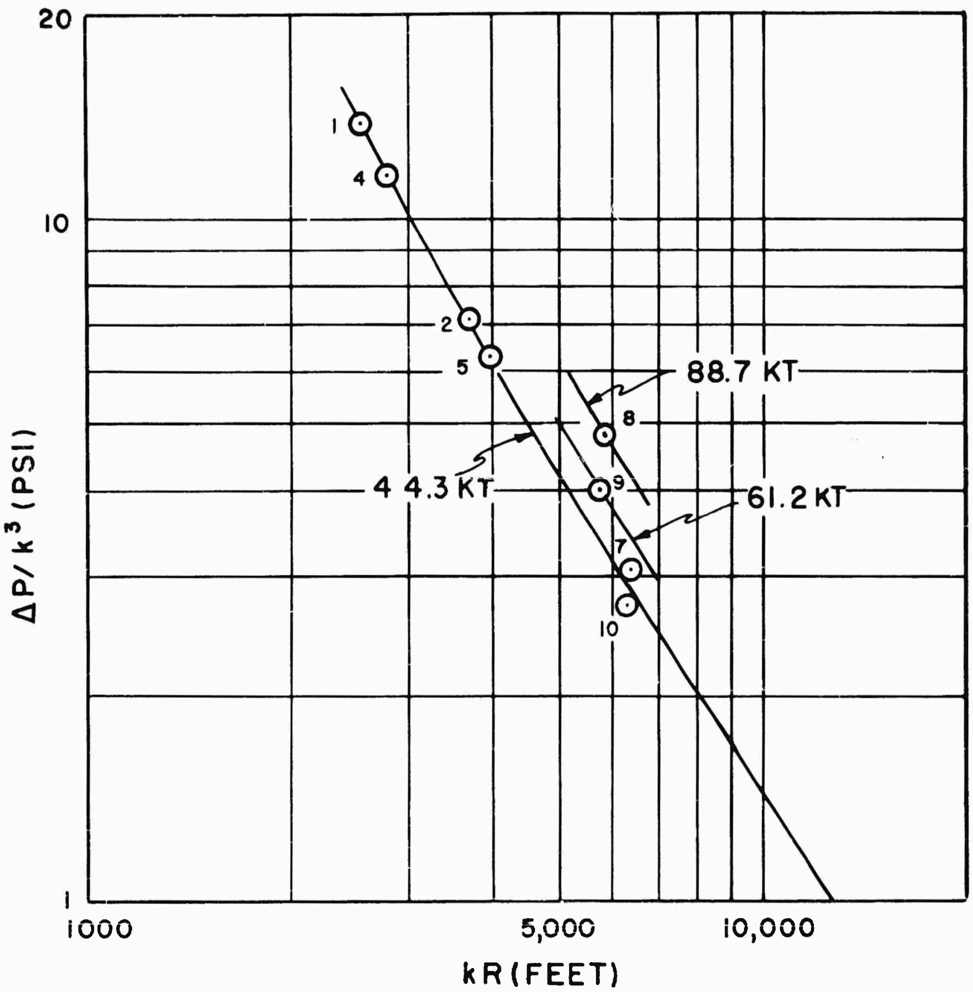

Figure 3.2 Shot 4 peak overpressure versus slant range reduced to sea level.

14.70 psi. The reduced data points have been fitted to the sea level free air overpressure versus distance curve of Reference 6. Optimum fit for the canisters in the free air region is obtained for an assumed yield of 44.3 kt, which is in satisfactory agreement with the currently accepted value of 43 ±2 kt. The peak overpressure at canister 8 is equivalent to a free-air yield of 88.7 kt, giving an apparent Mach reflection factor of 88.7/44.3 = 2.00 at this point. For canister 9 the equivalent free-air yield is 61.2 kt and the corresponding Mach reflection factor is 1.38. This decrease in the

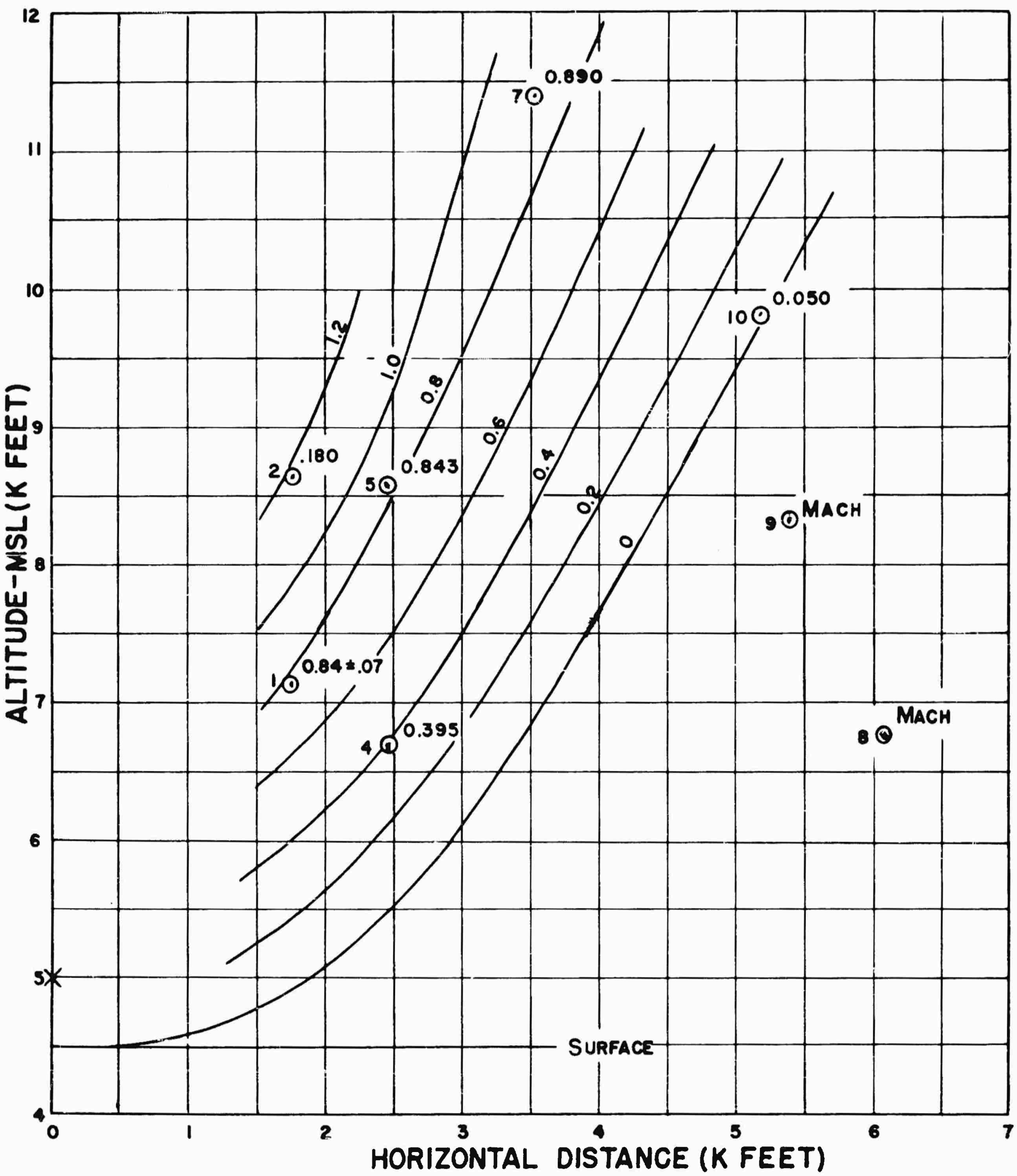

Figure 3.3 Shot 4 lines of equal reflection time intervals.

apparent reflection factor as the point of observation moves upward along the Mach shock, together with the small amplitude of the reflected shock in the free-air region, suggests that the reflected shock is refracted outward and probably strongly attenuated in passing back through the fire-ball region of high temperatures and large temperature gradients.

In Figure 3.3, an attempt is made to generalize the observed data on the time interval, T_2-T_1, between the direct and reflected shocks in the form of a contour plot of equal values of T_2-T_1. The ordinates in this figure are altitudes above sea level, and the abscissae are horizontal radial distances from a vertical axis through the shot. Strictly speaking, the axis of symmetry for a plot of this kind should be taken along the normal to the reflecting surface. However, no correction for the slope of the terrain has been made in this case since the mean slope is only 1.6 degrees (downward in azimuth 100 degrees), and the correction would be negligible compared to the uncertainty involved in constructing a contour plot on the basis of so small a number of control points. Shock photography by Project 1.2 shows indications of a second shock overtaking the primary shock directly above the shot at an altitude between 7,250 feet and 7,550 feet MSL. If this is in fact the same second shock that appears on the canister records, the contours shown in Figure 3.3 must turn up sharply between the canister 2 position and the vertical axis. However, since the second shock detected photographically appears to propagate with an inexplicably high velocity, there is some question as to the physical interpretation of the photographic image, and extrapolation of the contours of Figure 3.3 toward the vertical axis is not considered advisable.

3.2 SHOT 8

Canister coordinates with respect to ground zero at shock arrival time are given in Table 3.3. As in the case of Shot 4, they have been corrected for drift and fall during shock travel time from the zero time photographic coordinates.

Tracings of the telemetered overpressure-versus-time curves are shown in Figure 3.4. In this case reflected shocks appear on the records from all canisters. The observed peak overpressures, corrected peak overpressures, and arrival times are given in Table 3.4. Peak overpressure of the first shock reduced to standard sea-level conditions is plotted against reduced slant range in Figure 3.5. The solid curve shown in the figure is computed from the sea-level, free-air, overpressure-versus-distance curve of Reference 6 for a yield of 17.6 kt, which best fits the canister data. This is slightly higher than the currently accepted value of 15 ±2 kt.

Values of the time interval between direct and reflected shocks are presented in the form of a contour plot against altitude and horizontal range in Figure 3.6. The terrain beneath Shot 8 has a mean slope of about 1.8 degrees (downward in azimuth 96.5 degrees),

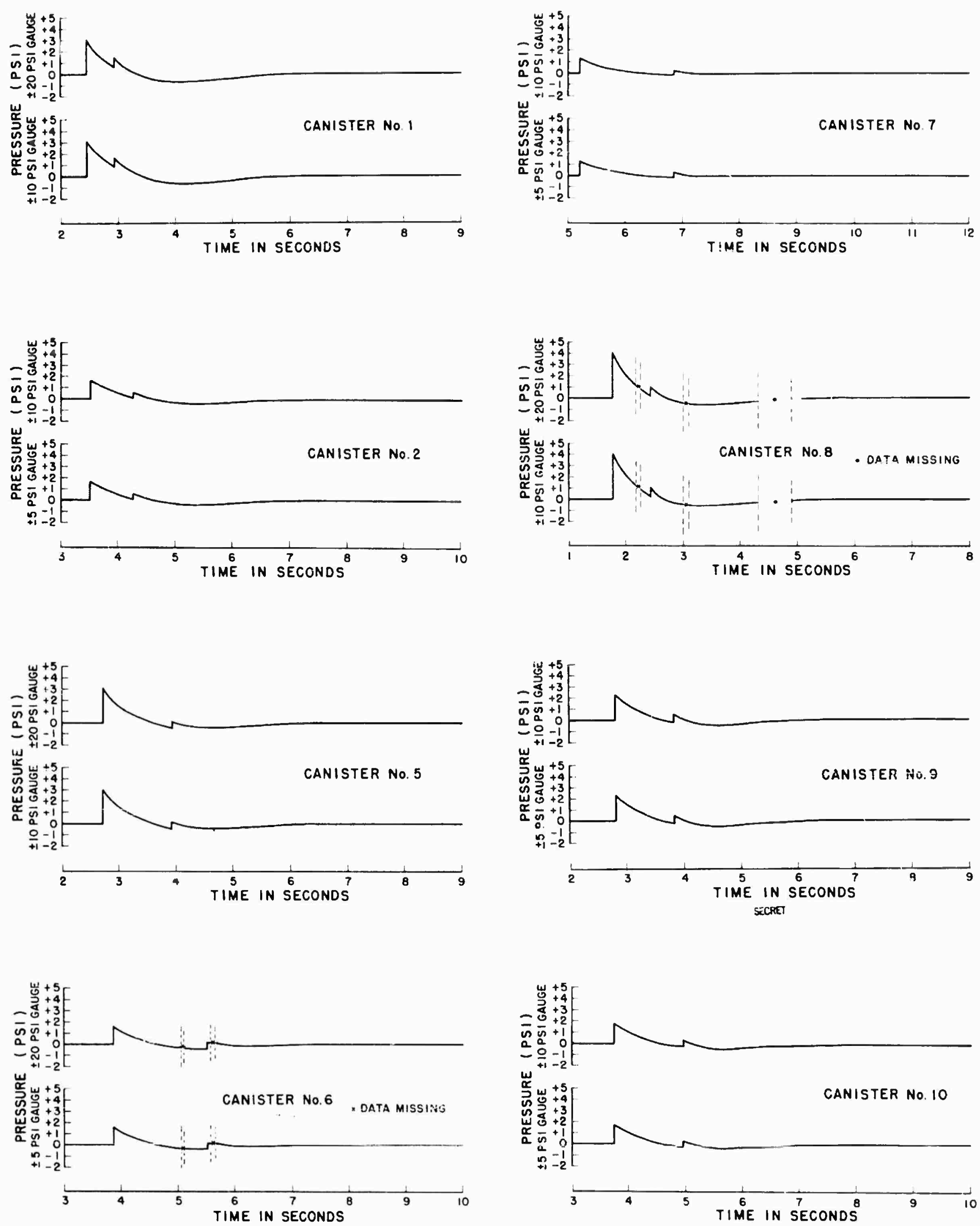

Figure 3.4 Shot 8 pressure versus time curves.

but as in the case of Shot 4 no correction has been applied for the small inclination of the axis of symmetry caused by this slope.

3.3 COMPARISON OF TELEMETERING AND SELF-RECORDING GAGES

The readings of peak overpressure of the direct and reflected shocks and the time interval between them as obtained from the telemetered records and from the self-recording mechanical gages are compared in Table 3.5. The pressure input to the self-recording gages was not taken off the same probe that transmits the external pressure to the telemetering gages, but was fed from four ports spaced at 90-degree intervals around the body of the canister. Flow effects would therefore not be the same for the two gages.

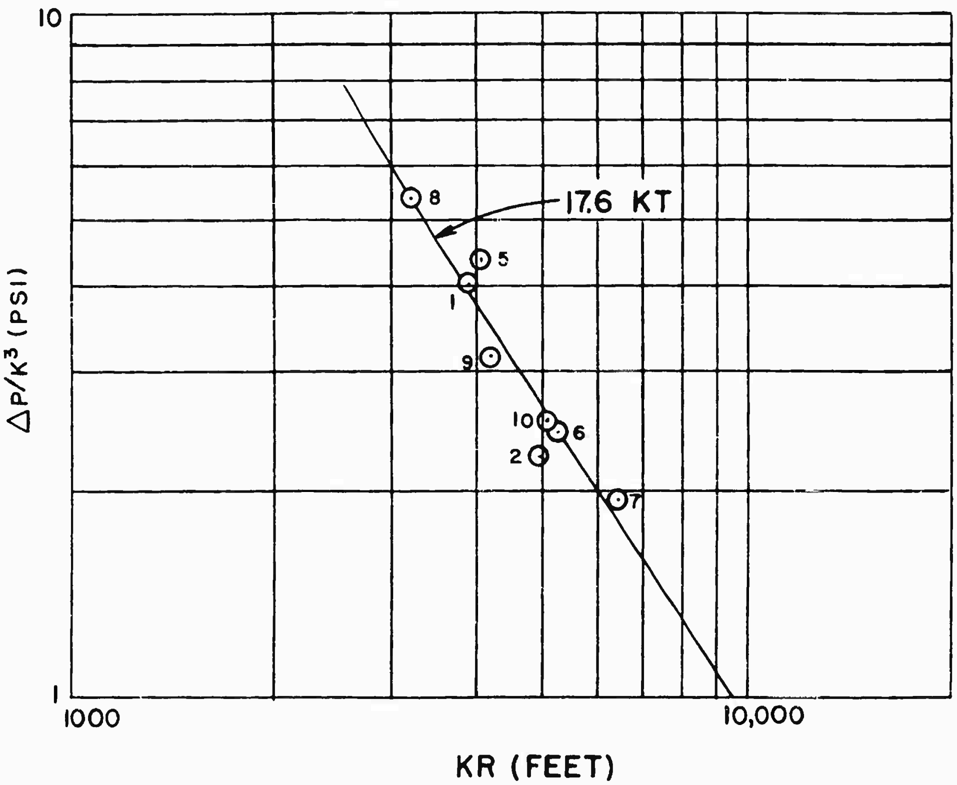

Figure 3.5 Shot 8 peak overpressure versus slant range reduced to sea level.

However, since the shock strength was comparatively small at all the canisters from which both telemetered and self-recorded data were obtained, the correction for flow effects could not be large in either case so that the comparison between the uncorrected readings shown in Table 3.5 is considered satisfactory.

No telemetered signal was received from canister No. 3 on Shot 8; therefore no comparison is possible in this case.

3.4 SHOT 10

Canister positions with respect to a ground coordinate system were determined by EG+G from photographs taken at two second

TABLE 3.1 CANISTER LOCATIONS AT SHOCK ARRIVAL TIME FOR SHOT 4

Canister	X (Feet)	Y (Feet)	$(X^2 + Y^2)^{\frac{1}{2}}$ (Feet)	Altitude (Feet MSL)	Slant Range (Feet)
1	-426	1,700	1,752	7,132	2,766
2	-130	1,765	1,770	8,643	4,058
4	-448	2,419	2,460	6,692	2,991
5	-203	2,454	2,463	8,592	4,361
7	137	3,523	3,526	11,407	7,320
8	113	6,068	6,069	6,769	6,324
9	332	5,376	5,386	8,319	6,331
10	362	5,160	5,173	9,819	7,075

Note: +X East and +Y North

TABLE 3.2 PEAK OVERPRESSURES AND ARRIVAL TIMES FOR SHOT 4

Canister	P_o (psi)	ΔP_g (psi)	ΔP_1 (psi)	T_1 (sec)	ΔP_2 (psi)	T_2 (sec)
1	11.47	9.25	10.36	1.081	0.75	1.91±.07
2	10.85	4.88	5.27	2.006	.77	3.186
4	11.63	7.99	9.11	1.241	1.99	1.636
5	10.86	4.35	4.61	2.187	.88	3.030
7	9.76	1.95	2.03	4.777	.33	5.667
8	11.60	3.50	3.78	3.770	---	---
9	10.98	2.88	3.00	3.914	---	---
10	10.37	1.88	1.90	4.469	0.10	4.519

P_o - Ambient pressure in psi obtained from meteorological data taken at shot time
ΔP_g - Peak overpressure (psi) of direct shock wave as indicated by gage
ΔP_1 - Peak overpressure (psi) of direct shock wave corrected by shock tube calibration
T_1 - Arrival time (sec) of direct shock wave
ΔP_2 - Peak overpressure (psi) of reflected shock wave
T_2 - Arrival time (sec) of reflected shock wave

TABLE 3.3 CANISTER LOCATIONS AT SHOCK ARRIVAL TIME FOR SHOT 8

Canister	X (Feet)	Y (Feet)	$(X^2 + Y^2)^{\frac{1}{2}}$ (Feet)	Altitude (Feet MSL)	Slant Range (Feet)
1	2,478	2,103	3,250	7,476	4,200
2	2,933	1,994	3,547	8,930	5,432
5	396	1,864	1,905	8,872	4,481
6	585	1,484	1,595	10,535	5,937
7	1,338	1,601	2,087	11,963	7,445
8	-1,830	1,655	2,468	7,225	3,449
9	-1,682	1,653	2,357	8,766	4,600
10	-1,818	1,381	2,282	10,024	5,686

Note: +X East and +Y North

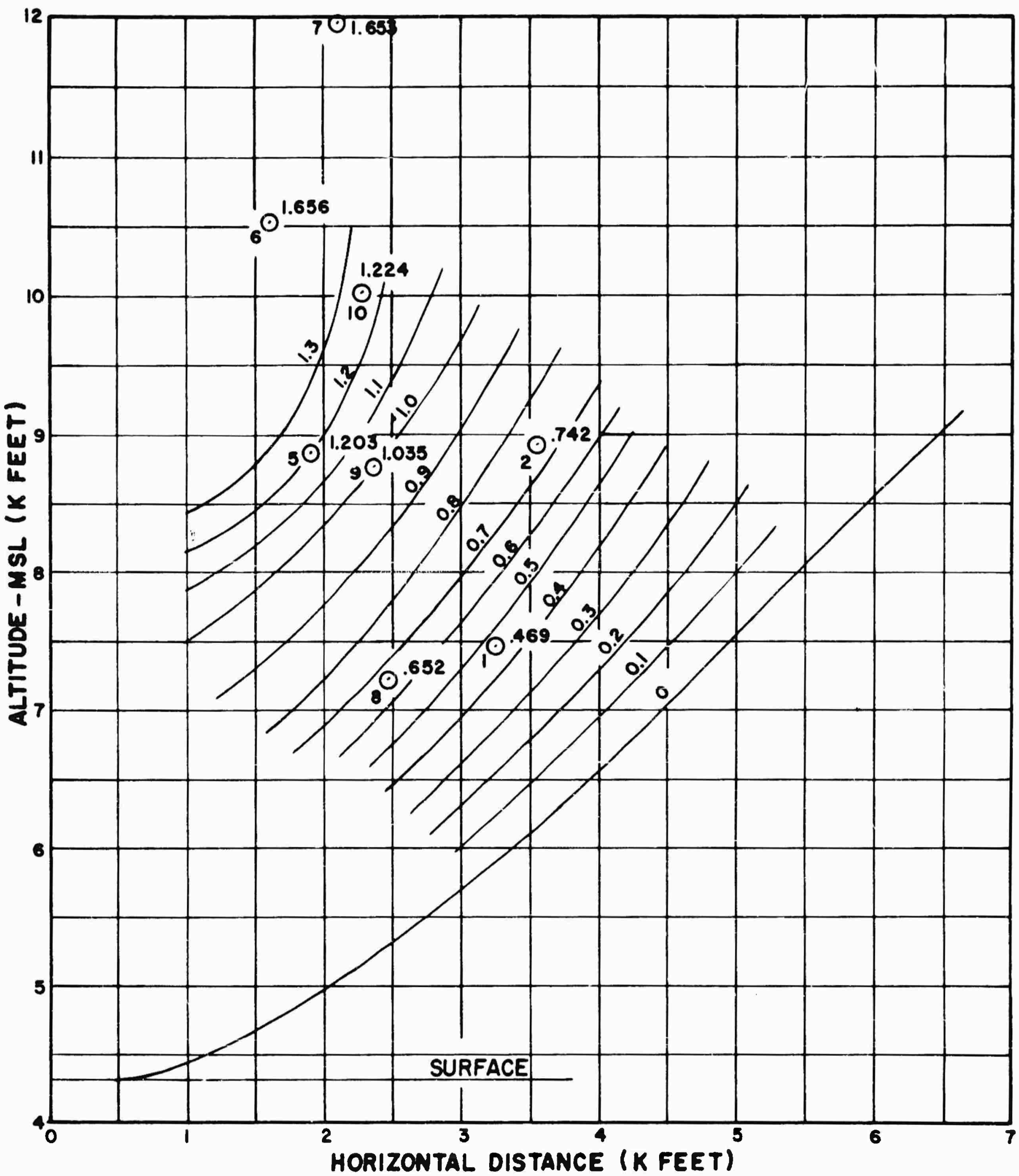

Figure 3.6 Shot 8 lines of equal reflection time intervals.

intervals from H minus four seconds to H plus ten seconds. Since the shock wave, as well as the canisters, is convected horizontally with the ambient wind, the effective canister slant ranges at shock arrival time should be taken with reference to a coordinate system moving with the wind. These may be obtained by taking the horizontal coordinates to be those measured at zero time (since the canister trajectories at that time would be essentially vertical

TABLE 3.4 PEAK OVERPRESSURES AND ARRIVAL TIMES FOR SHOT 8

Canister	P_o (psi)	ΔP_g (psi)	ΔP_1 (psi)	T_1 (sec)	ΔP_2 (psi)	T_2 (sec)
1	11.18	3.00	3.08	2.470	0.75	2.939
2	10.59	1.60	1.62	3.520	0.40	4.262
5	10.60	3.00	3.15	2.720	0.55	3.923
6	9.96	1.60	1.66	3.878	0.50	5.534
7	9.44	1.20	1.25	5.204	0.38	6.857
8	11.28	4.00	4.12	1.768	0.80	2.420
9	10.65	2.20	2.27	2.804	0.60	3.839
10	10.17	1.70	1.75	3.741	0.45	4.965

P_o - Ambient Pressure (psi) obtained from meteorological data taken at shot time
ΔP_g - Peak overpressure (psi) of direct shock wave as indicated by gage
ΔP_1 - Peak overpressure (psi) of direct shock corrected by shock tube calibration
T_1 - Arrival time (sec) of direct shock wave
ΔP_2 - Peak overpressure (psi) for reflected shock wave
T_2 - Arrival time (sec) of reflected shock wave

TABLE 3.5 COMPARISON OF TELEMETERING AND SELF-RECORDING GAGES

Shot	Array Position No.		Telemetered	Self-Recording Gage
4	7	1st Peak Overpressure	1.95	1.87 psi
4	7	2nd Peak Overpressure	0.33	0.32 psi
4	7	$T_2 - T_1$	0.890	0.877 sec
4	8	1st Peak Overpressure	3.50	3.30 psi
8	1	1st Peak Overpressure	3.00	2.75 psi
8	1	2nd Peak Overpressure	0.75	0.45 psi
8	1	$T_2 - T_1$	0.469	0.474 sec
8	3	1st Peak Overpressure	---	5.96 psi
8	3	2nd Peak Overpressure	---	0.78 psi
8	7	1st Peak Overpressure	1.20	1.10 psi
8	7	2nd Peak Overpressure	0.38	0.43 psi
8	7	$T_2 - T_1$	1.653	1.653 sec

TABLE 3.6 EFFECTIVE CANISTER COORDINATES RELATIVE TO BURST, SHOT 10

Canister No.	X (Feet)	Y (Feet)	(z-h) (Feet)	R (Feet)
4	-805	470	115	939±36
5	-955	590	330	1,126±39
6	-1,200	765	380	1,473±37
7	-1,330	690	455	1,566±41
8	-1,615	940	605	1,964±41
9	-2,050	1,230	705	2,492±40
10	-2,510	1,355	890	2,988±41
11	-3,025	1,725	830	3,580±38
13	-5,920	3,285	1,545	6,944±43
14	-7,955	4,410	2,285	9,378±42
15	-9,975	5,600	3,090	11,849±46

X = Positive to East
Y = Positive to North
z-h = Elevation of Canister above Burst Altitude
R = Slant Range
Burst Altitude = 36,645 feet MSL

except for wind drift) and taking the vertical coordinates to be those obtained by interpolating to shock arrival time between the times of the EG+G photographic measurements. The effective coordinates and slant ranges with respect to the burst, defined in this way, are given in Table 3.6.

From the differences between independent measurements of the canister coordinates EG+G assign a standard deviation of ±20 feet in the North coordinates (y) and ±25 feet in the East coordinates (x) at zero time. The standard deviation in the measurement of altitude at shock arrival time varies with position in the array from about ±60 feet at canister 4 to ±120 feet at canister 15. A readable image of the burst appeared on only two films so that only a single measurement of the burst coordinates could be made. Therefore the accuracy of the burst coordinates cannot be checked by independent measurements, but EG+G estimate on the basis of the consistency of the canister measurements that the burst coordinates are known to standard deviations of ±20 feet in the North coordinate, ±25 feet in the East coordinate, and ±30 feet in altitude. Since the slant ranges cannot be measured directly, the errors in slant range must be estimated from the standard deviations of the coordinates by the usual method of propagation of errors, treating the errors in burst coordinates and canister coordinates as statistically independent. The standard deviations in slant range tabulated in Table 3.6 are obtained in this way. From the deviations between independent measurements of the slant ranges between adjacent canisters, EG+G estimate standard deviations in slant range of ±25 feet at zero time and ±45 feet at shock arrival time. The latter figure is comparable to the values given in Table 3.6.

The telemetered overpressure-versus-time curves are reproduced in Figure 3.7. These have been corrected for baseline drift (assumed linear) caused by canister descent after shock arrival and the sealing of the pressure reference chamber.

Peak overpressures, as read and as corrected according to the BRL shock-tube calibration, shock-arrival times, and positive-phase duration are given in Table 3.7. Modified Sachs scaling has been used to reduce the corrected peak overpressures and slant ranges to equivalent values at shot altitude using the meteorological data for shot time tabulated in Appendix A. The reduced values are plotted in Figure 3.8 together with the lower end of the high overpressure-versus-distance curve determined from shock photography by Project 1.2 (Reference 7). The agreement in the region of overlap is considered highly satisfactory. The curve shown by the dashed line in Figure 3.8 is computed for 3.3 kt, the currently accepted radio-

TABLE 3.7 OBSERVED DATA SHOT 10

Canister No.	ΔP_g (psi)	ΔP (psi)	T (sec)	T+ (sec)
4	7.90	12.3	0.220	---
5	4.78	6.95	0.359	0.304
6	2.70	3.43	0.570	0.392
7	2.45	3.05	0.630	0.425
8	1.62	1.88	0.941	0.466
9	1.12	1.24	1.380	0.525
10	0.860	0.939	1.810	0.576
11	0.720	0.770	2.338	0.670
13	0.266	0.274	5.495	0.806
14	0.166	0.169	7.830	0.906
15	0.120	0.122	10.244	0.980

ΔP_g - Peak overpressure as indicated by gage
ΔP - Peak overpressure corrected by shock tube calibration
T - Time of shock arrival
T+ - Duration of positive overpressure phase

TABLE 3.8 COMPARISON OF OBSERVED AND SCALED TIMES-OF-ARRIVAL REDUCED TO SHOT ALTITUDE

Canister No.	Slant Range	Time-of-Arrival	
		Observed	Scaled from WT-710 and TM23-200 for 3.3 kt at Shot Altitude
	(feet)	(sec)	(sec)
4	936±36	.219	.228±.017
5	1119±39	.357	.327±.023
6	1464±37	.567	.546±.028
7	1553±41	.625	.605±.031
8	1946±41	.933	.898±.034
9	2465±40	1.365	1.317±.034
10	2946±40	1.785	1.73 ±.037
11	3533±38	2.308	2.20 ±.034
13	6784±42	5.369	5.27 ±.042
14	9030±40	7.548	7.45 ±.039
15	11292±44	9.783	9.63 ±.045

TABLE 3.9 TIMES-OF-ARRIVAL CALCULATED FROM OBSERVED PEAK OVERPRESSURES REDUCED TO SHOT ALTITUDE

Canister No.	Rankine-Hugoniot Velocity		Range Increment	Time Increment	Time-of-Arrival
	Instantaneous	Interval			
	(ft/sec)	(ft/sec)	(ft)	(sec)	(sec)
4	2050				.219
		1864	183	.0982	
5	1678				.317
		1525	345	.2262	
6	1372				.543
		1354	89	.0657	
7	1336				.609
		1276	393	.3080	
8	1216				.917
		1180	519	.4398	
9	1144				1.357
		1126	481	.4272	
10	1108				1.784
		1098	587	.5346	
11	1087				2.319
		1056	3251	3.0786	
13	1025				5.397
		1019	2247	2.2051	
14	1012				7.602
		1009	2261	2.2408	
15	1006				9.843

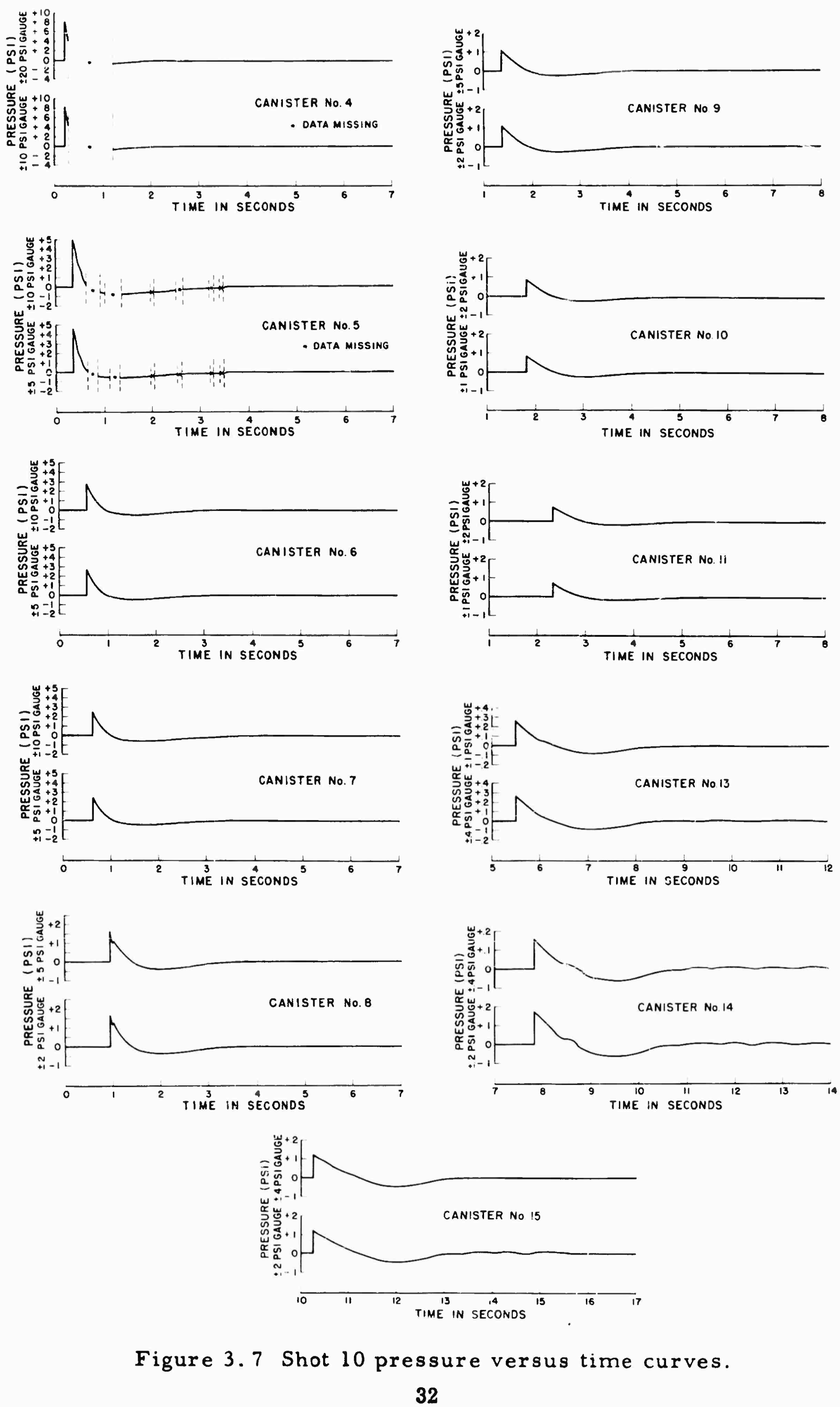

Figure 3.7 Shot 10 pressure versus time curves.

chemical yield, at shot altitude (36,645 ± 30 feet MSL, ambient pressure 222 mb) by applying Sachs scaling to the overpressure-versus-distance curve tabulated in Reference 6.

Positive phase duration is plotted against slant range, both reduced to shot altitude, in Figure 3.9. The comparison curve shown in this Figure is derived by Sachs scaling the positive-duration curve of the recent revision of TM 23-200, "Capabilities of Atomic Weapons," to 3.3 kt at shot altitude. Because of the motion of the canisters under the combined effects of gravity and drag forces after shock-arrival time, the interpretation of the apparent positive phase duration as recorded by the canisters is somewhat questionable; therefore, conclusions will not be drawn on the scaling of altitude effects from the comparisons shown in Figure 3.9.

With the standard deviations in slant range given in Table 3.6, the peak overpressures computed directly from the observed interval velocities by means of the Rankine-Hugoniot equation are uncertain by factors varying from about 1.6 to ten and therefore have little meaning. However, there is some value in an over-all comparison of the observed travel times with those calculated by scaling from the Upshot-Knothole, Tumbler, Ivy composite time-of-arrival curve for 1 kt at sea level given in Reference 10 and its extension to longer ranges given in TM 23-200. This comparison is shown in Table 3.8 which gives the canister slant ranges and their estimated standard deviations reduced by modified Sachs scaling to shot altitude, the observed times-of-arrival similarly scaled to shot altitude, and the times-of-arrival computed by Sachs scaling to 3.3 kt at shot altitude from the standard curves referred to above. The standard deviations tabulated with the computed times-of-arrival are those corresponding to the tabulated standard deviations in range and do not include any additional uncertainties due to errors in the value of sound velocity at shot altitude and non-uniformity in wind velocity over the range of shot and canister altitudes. Out to canister 7 the difference between the observed and computed times-of-arrival is less than the standard deviation of the latter, but beyond canister 8 the observed times are greater than the computed times by more than the standard deviation. This trend is in agreement with the observation that the peak overpressures fall below the reference curve at intermediate distances, as shown in Figure 3.8. From canister 8 through canister 15 the observed times-of-arrival average 2.9 percent greater than the computed times-of-arrival. An error of one degree in the ambient temperature represents an error of only 0.17 percent in ambient sound velocity, so that errors attributable to this source are probably negligible. The method of computing effective slant ranges that we have used implicitly assumes

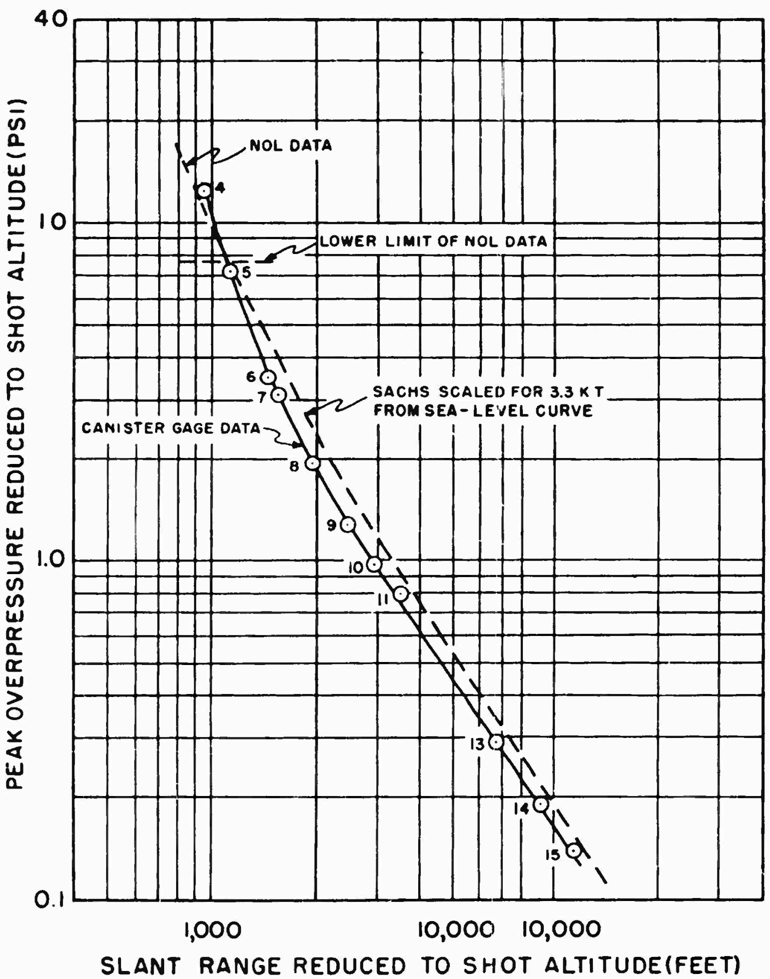

Figure 3.8 Shot 10 peak overpressure versus slant range reduced to shot altitude.

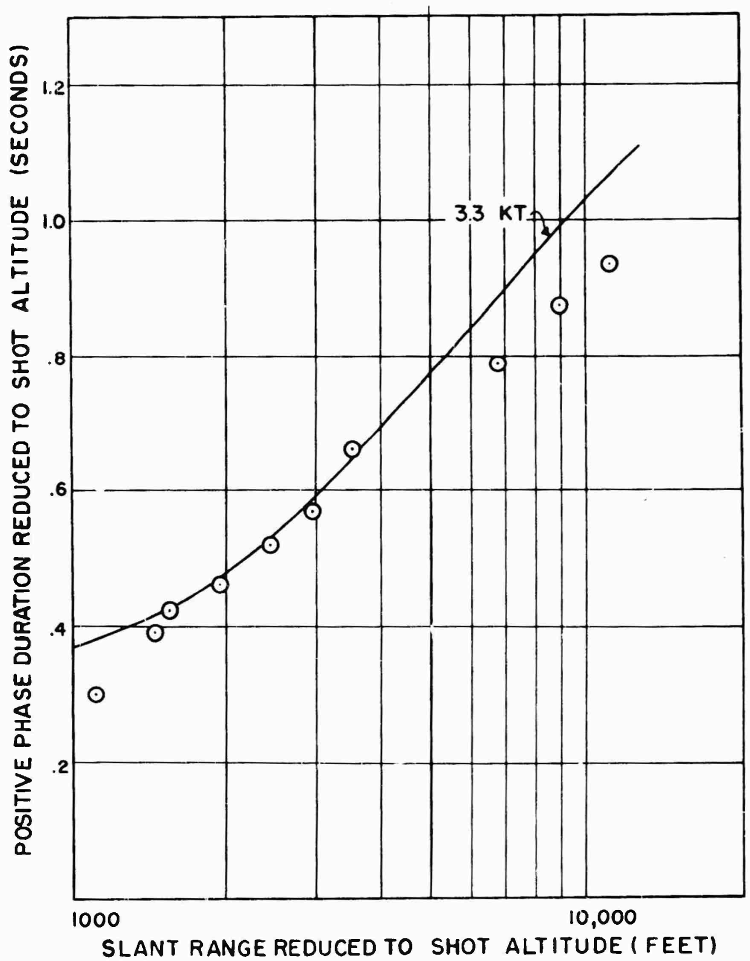

Figure 3.9 Shot 10 positive phase duration versus slant range reduced to shot altitude.

that the wind is constant in direction and magnitude over the range of altitudes between shot and canister. In actuality, the meteorological data shows the wind velocity increasing from 48 ft/sec at shot altitude to 71 ft/sec at the altitude of canister 15. The variation from the mean thus amounts at most to ±12 ft/sec, or 1.2 percent of ambient sound velocity. It does not, therefore, appear likely that errors due to non-uniformity of the wind can account for the differences between observed and calculated times-of-arrival.

As an alternative test for consistency between the measured peak overpressures and times-of-arrival we may use the observed peak overpressures to calculate the shock velocity, U, at each canister according to the Rankine-Hugoniot equation

$$U = c_o \left(1 + \frac{6}{7} \frac{\Delta P}{P_o} \right)^{1/2} \tag{3.1}$$

and then integrate numerically from the observed time at canister 4 to determine the corresponding calculated times-of-arrival at all other canisters. In performing the numerical integration it is assumed that the average velocity of the shock wave over the interval between two adjacent canisters is equal, to a sufficiently good approximation, to the mean of the instantaneous velocities computed at the two canisters. To permit direct comparison with the times-of-arrival of Table 3.8, the observed peak overpressures and slant ranges reduced to shot altitude, and the value of sound velocity at shot altitude, 985.7 ft/sec, are used in the computations. Thus the times-of-arrival, like those tabulated in Table 3.8, refer to an equivalent horizontal array at shot altitude. The results are presented in Table 3.9. Except for canisters 5, 14, and 15 the differences between the observed and computed times-of-arrival are less than the standard deviations corresponding to the estimated uncertainties of the slant ranges. At canisters 14 and 15 the discrepancies amount to only 0.7 and 0.6 percent of the computed times-of-arrival respectively. We therefore conclude that the observed peak overpressures and times-of-arrival are mutually consistent to a satisfactory degree.

Chapter 4
CONCLUSIONS and RECOMMENDATIONS

4.1 SHOTS 4 AND 8

Although the positions actually attained by the canisters at shock arrival time did not provide any direct information on the distribution of overpressure along the vertical axis above the shot, the very small amplitude of the reflected shock observed at points off the vertical suggests that if the reflected shock does overtake the direct shock above the shot, it will result in only a small increase in peak overpressure. Presumably this is due to strong attenuation or divergence of the reflected shock in passing back through the high temperature region of the fireball, since in the Mach region well below the triple point the overpressures observed on Shot 4 are considerably greater than the free air value. Because of the unexpectedly low yield of Shot 8, this shot contributed little information on the locus of fusion of the direct and reflected shocks for low, scaled heights of burst.

Analysis of the canister positioning errors in the light of the data on the wind structure existing at drop time indicates that a very large part of the positioning errors (nearly all of it in the case of Shot 8) arises from the computation of the wind drift correction on the basis of data taken about 3 hours before shot time. Unless the winds are unusually constant, this error is practically unavoidable, and it is therefore recommended that in any future operations of this kind, where positioning is critical, a much larger number of canisters should be dropped. The performance of the self-recording gages tested at Shots 4 and 8 is considered satisfactory, and their use in a large array of small canisters is recommended for future tests at the NTS, where recovery is not a serious problem.

4.2 SHOT 10

In assessing whether the Shot 10 results do or do not indicate a significant departure from Sachs scaling at high altitudes it should be borne in mind that the comparison curve shown in Figure 3.8 is only an estimate of a reasonable, most-probable curve and that the experimental data obtained at lower altitudes shows a rather wide statistical distribution about this curve. The curves shown in Figure 4.1 represent, on a 1-kt-at-sea-level basis, the upper and

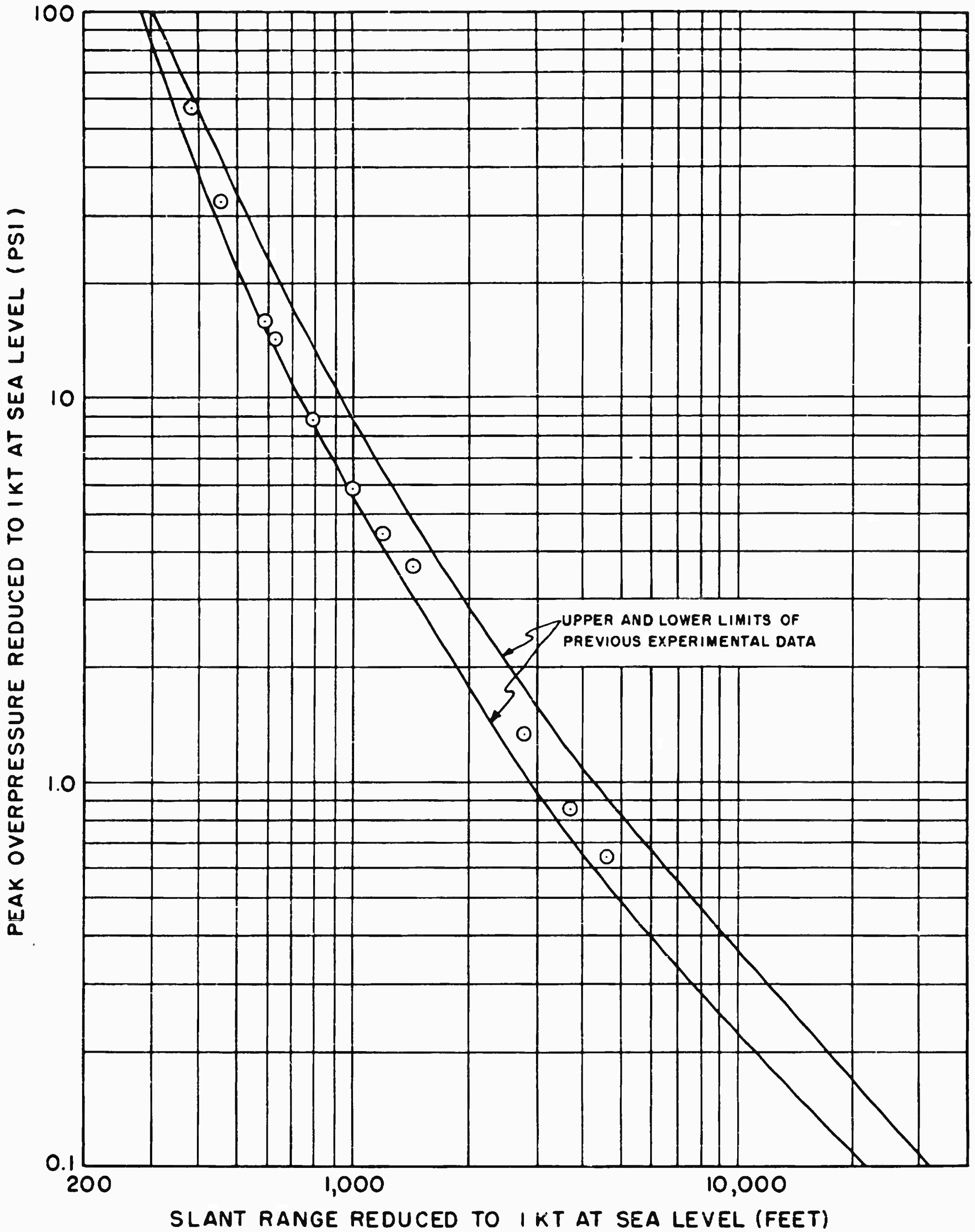

Figure 4.1 Shot 10 peak overpressure versus slant range reduced to 1 kt at sea level.

lower limits which would include essentially all the free-air, peak-overpressure measurements obtained by all methods at Tumbler Shots 1, 2, 3, and 4 (Reference 8), Ivy King (Reference 9), and Upshot-Knothole Shots 1, 4, and 9 (References 10 and 11). If the shock photography data of Greenhouse Shot George were included, the upper limit would have to be considerably increased above the 30-psi level. It is believed that the width of this band of variation should not be attributed entirely to errors of measurement or methods of data reduction, but that a considerable part of it comes from real variations from one shot to another in the early development of the blast wave and, increasingly at lower overpressures, unpredictable effects of winds, turbulence, and atmospheric temperature fluctuations. The Shot 10 canister data scaled to 1 kt at sea level (modified Sachs scaling using 3.3 kt for yield) are tabulated in Table 4.1 and plotted in Figure 4.1. Since all the Shot 10 points fall within the extreme range of variability indicated by previous experience, it is not thought that the variation from the mean curve should be interpreted as indicating a real departure from Sachs scaling which would be found to hold for all shots at altitudes comparable to that of Shot 10.

TABLE 4.1 SHOT 10 PEAK OVERPRESSURE VERSUS SLANT RANGE REDUCED TO 1 KT AT SEA LEVEL

Canister No.	Pressure Scale Factor $14.70/P_o(z)$	Range Scale Factor $[P_o(z)/14.70W]^{1/3}$	Scaled Overpressure (psi)	Scaled Slant Range (Feet)
4	4.605	.4124	56.6	387
5	4.647	.4111	32.3	463
6	4.647	.4111	15.9	606
7	4.668	.4103	14.2	643
8	4.690	.4099	8.82	805
9	4.712	.4091	5.84	1,019
10	4.756	.4078	4.47	1,219
11	4.734	.4082	3.65	1,461
13	4.894	.4041	1.34	2,806
14	5.116	.3983	.864	3,735
15	5.276	.3942	.644	4,671

Appendix A
METEOROLOGICAL DATA

TABLE A.1 METEOROLOGICAL DATA, SHOT 4, 0520 PST, 7 MARCH 1955

Height (Kft)	Wind (deg/kts)	Pressure (mb)	Temp (°C)
SFC	290/06	892	3.9
4	310/10	886	4.1
5	010/19	854	5.9
5.213	---	850	6.0
5.446	---	842	6.2
6	030/21	815	5.2
6.693	---	802	3.4
7	030/20	795	3.8
8	050/15	767	3.9
8.760	---	744	4.0
9	030/07	738	3.9
10	360/02	710	2.2
10.381	---	700	1.7
11	310/02	684	0.7
12	130/04	657	-1.2
13	140/06	633	-3.1
14	130/07	606	-5.5
15	140/06	585	-7.3
16	090/04	563	-9.4
17	070/06	541	-11.7
18	070/08	521	-13.4
18.986	---	500	-15.5
19	050/13	499	-15.6
20	050/14	480	-17.8
21	050/11	459	-20.0
21.555	---	450	-22.0
22	060/09	441	-22.7
23	070/08	422	-25.6

TABLE A.2 METEOROLOGICAL DATA, SHOT 8, 0510 PST, 29 MARCH 1955

Height (Kft)	Wind (deg/kts)	Pressure (mb)	Temp (°C)
SFC	270/02	880	0.5
4	260/03	878	1.5
4.360	---	865	9.1
4.860	---	850	9.3
5	200/09	846	9.3
5.150	---	840	9.3
5.910	---	817	7.6
6	180/12	813	7.3
7	190/16	784	5.3
8	190/20	756	3.6
8.270	---	746	3.0
9	190/22	728	2.4
10	190/19	702	1.5
10.060	---	700	1.5
10.930	---	677	0.8
11	200/15	675	1.0
11.610	---	660	2.0
12	240/15	650	1.0
13	260/21	626	-1.2
14	260/23	603	-3.4
14.210	---	597	-4.0
15	260/19	580	-6.2
16	260/20	557	-9.0
17	260/24	536	-11.7
18	260/27	515	-14.5
18.710	---	500	-16.4
19	270/31	495	-17.2
20	270/34	475	-20.0
21	270/36	456	-22.6
22	270/36	436	-25.4
23	270/33	418	-28.2
24	270/34	402	-30.9
24.070	---	400	-31.1
25	270/38	383	-33.6

TABLE A.3 METEOROLOGICAL DATA, SHOT 10, 1000 PST, 6 APRIL 1955

Height (Kft)	Wind (deg/kts)	Pressure (mb)	Temp (°C)
SFC	030/09	885	10.5
---	---	---	---
34	320/29	249	-46.8
35	320/27	238	-47.2
36	300/28	228	-47.6
37	300/29	218	-48.0
38	300/31	209	-48.2
38.806	---	200	-47.3
39	300/38	198	-47.0
40	290/43	190	-45.9
40.223	---	188	-45.7
41	290/45	181	-46.0
42	290/47	173	-46.8
43	290/47	166	-48.6
44	300/45	158	-50.9
45	300/44	151	-52.4
45.023	---	150	-52.5
46	300/40	143	-53.8

Appendix B
SHOCK TUBE CALIBRATION OF PRESSURE PROBE

B.1 BACKGROUND ON PROBE DESIGN

When plans for air-borne blast-pressure measurements were being made before Operation Jangle, it was anticipated that the instrumentation under consideration would not, in general, be used to measure shocks of strength greater than that equivalent to about 5-psi overpressure at sea level, i.e., a ratio of peak overpressure to ambient pressure of 0.34. At this overpressure ratio, the perturbation of the free-field pressure caused by the presence of a pressure-pick-up probe cannot be extremely large, since the peak dynamic pressure, $(1/2)\rho v^2$, is only 0.116 times the peak static overpressure. Also, since the angle of incidence of the shock front on the canisters was expected to vary over a wide range, a probe which would be relatively insensitive to orientation was desired. It was therefore decided to conduct the external pressure to the gages through tubing connected to the interior of a perforated spherical shell, with the idea that the pressure registered by the gage diaphragm would be effectively the mean pressure over the surface of the sphere and that this mean would differ by a negligible amount from the unperturbed free-field pressure. Relatively low-frequency gages were chosen in order to suppress the short-duration spike caused by shock reflection from the canister nose. After some preliminary tests with 5-psi shocks at one atmosphere ambient pressure in the BRL shock tube, the pressure probe adopted and used in Operation Jangle and Snapper was constructed in the form of a 2-inch-diameter spherical shell perforated with one hundred uniformly spaced, 0.080-inch-diameter holes. This sphere was mounted on the end of a slender cone 24 inches long, which also served as the telemetering antenna, extending forward from the hemispherical nose of the canister.

At Operation Ivy it was desired to make thermal-radiation measurements on the blast-pressure canisters, and the mounting requirements of the thermocouple dictated redesign of the pressure probe-antenna. The original shock-tube tests, although not as conclusive as might have been desired, suggested that the nondirectional properties of the spherical probe were probably an unnecessary refinement at the low shock strengths used. The new probe designed to carry the thermocouple as well as the pressure input orifices was made in the form of a 1-inch-diameter cylinder 24 inches long, terminating in a cone of 39-degrees included angle. The external pressure was led into an interior tube through twenty-four 0.080-inch-diameter orifices with centers in a band from 2 3/8 inches to 3 1/8 inches behind the base of the cone tip. This probe was used in Operation Upshot-Knothole and Teapot as well as in Ivy.

B.2 POST-SHOT SHOCK TUBE CALIBRATION

As a result of the discrepancy between the gage and velocity peak overpressures noted in Section 2.2, a series of measurements were made from 2 to 10 June 1955 utilizing the BRL shock tube at the Aberdeen Proving Grounds. At high shock strengths, the error in the gage reading is probably dependent mainly on the Mach number of the flow behind the shock front and on the angle of incidence of the shock on the probe. Since the Mach number of the flow can be expressed as a function of the peak overpressure ratio, $\Delta P/P_o$, only and does not depend on the ambient temperature, it should not be necessary to duplicate the actual ambient temperature of Shot 10 in order to have a valid calibration. The temperature coefficient of the diaphragm gages is not a major consideration, since the canisters are internally heated up to the time of drop and are sufficiently insulated so that the temperature change is negligible during the time of fall.

A possible source of error in the shock-tube calibration data is the relatively short time scale of the shocks that can be produced in the tube. The high-frequency response of the canister gage system is limited, not by the natural frequency of the gage diaphragm or the finite band width of the FM sub-carrier channels, but by the frequency of oscillation of the column of air in the 2-foot (approximate) lead-in tubing from the pressure-input orifices to the gage chamber. This frequency is approximately 80 cps. Damping is introduced by the insertion of a constricting orifice within the lead-in tubing, but this must be held to a moderate value (of the order of 0.2 critical), in order to avoid an excessive rise time. This results in an output pressure-time function which overshoots and then executes small oscillations with diminishing amplitude about the true input wave form. In reading the records, a mean curve is faired through these damped 80-cycle oscillations and extrapolated back to shock-arrival time over the rise-time interval. In the case of the field records, the rate of decrease of pressure behind the shock front is sufficiently slow in relation to the 0.012-to-0.014-second period of the superimposed oscillations so that the mean curve can be simply drawn in with little room for subjective error.

In the shock tube tests, the wave forms were more complex and had a shorter duration, a more or less flat-topped or slowly decaying portion of about 0.010-second duration being succeeded by a more rapid rate of decrease of pressure. This change in slope of the pressure-time curve at a time comparable to the period of the superimposed oscillations introduces a complication in the extrapolation of the true input curve back to shock-arrival time; however, in many of the shock-tube shots the pressure wave form was also recorded by a cathode-ray oscilloscope camera utilizing a high-frequency piezo-

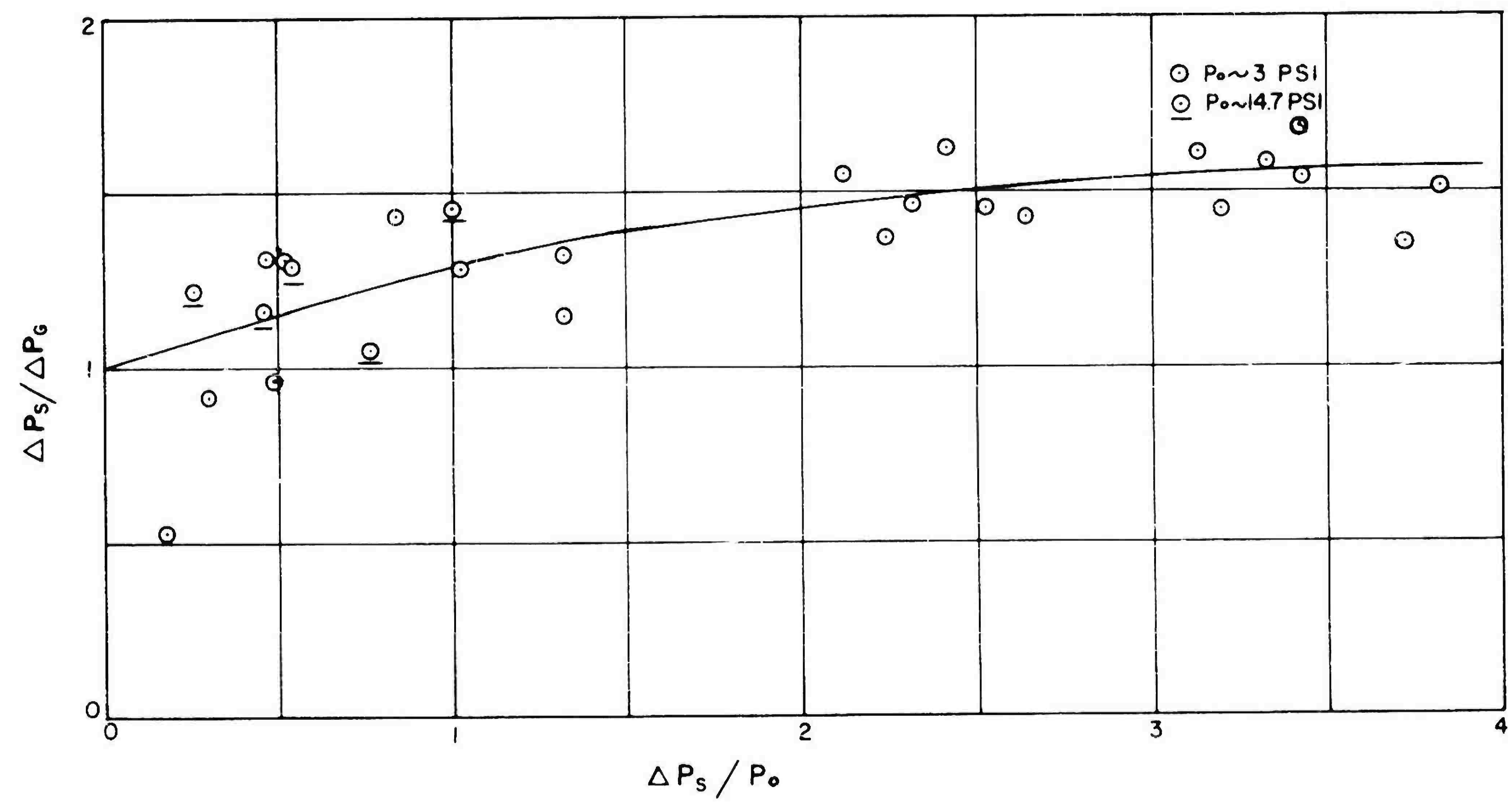

Figure B.1 Shock tube calibration of pressure probe. Axis of probe 90° to shock normal.

electric gage. It was assumed that these records give a relatively undistorted picture of at least the first 10 msec of the shock-tube wave; they were used as a guide in extrapolating the faired mean curve from the later portions of the low-frequency canister gage records back to shock-arrival time. Although it must be admitted that the peak gage overpressures (ΔP_g) resulting from this process of smoothing and extrapolation are subject to considerably more uncertainty than is the case with the field records, it is believed that this is random in nature and that the systematic effect of the air flow past the pressure probe is fairly well represented by the smoothed calibration curves.

For comparison with the peak gage overpressure, the actual shock overpressure (ΔP_s) was taken to be that computed by the Rankine-Hugoniot equation from the shock velocity as measured in the tube. The gage instrumentation was the same as that used in the field except that the telemetering link was eliminated.

A total of 66 usable shots were made. These are grouped in the following four categories:

1. With the axis of the pressure probe mounted at 90 degrees to the normal to the incident shock wave, measurements were made

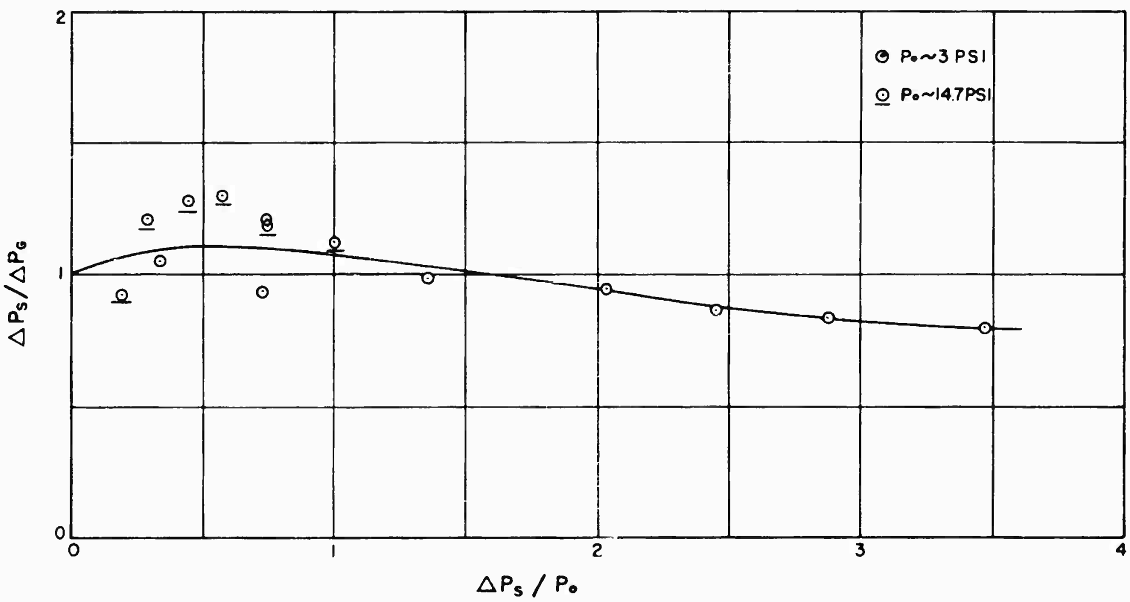

Figure B.2 Shock tube calibration of pressure probe. Axis of probe parallel to shock normal.

on 27 shots with overpressure ratios ranging from 0.17 to 3.82. Five of the above shots were performed with the expansion chamber at sea-level pressure and the rest with the expansion chamber at about 3 psi, which was near the ambient pressure at Shot 10. The results of these measurements are shown in Figure B.1. The overpressure ratio ($\Delta P_s/P_o$) is the abscissa, and the ratio ($\Delta P_s/\Delta P_g$) of the actual shock overpressure to the overpressure as measured by the Bendix gage is the ordinate. At low values of $\Delta P_s/P_o$, the accuracy of the velocity method of measuring peak overpressure becomes very poor, and the point at $\Delta P_s/P_o = 0.17$ is probably grossly in error.

2. With the probe oriented at 0 degrees or head on to the shock wave, 14 shots were made with pressure ratios varying from 0.19 to 3.47. Again, some of the shots were made with the expansion chamber at sea-level pressure. The results of these shots are shown in Figure B.2.

3. With the probe oriented at 45 degrees to the shock wave, 8 shots were made with pressure ratios varying from 0.96 to 3.7. The results are shown in Figure B.3.

4. With the probe at 45 degrees to the shock wave, shots were made with the expansion chamber at pressures representing sea level, 10,000, 20,000, 30,000, and 40,000 feet. Identical pressure gages

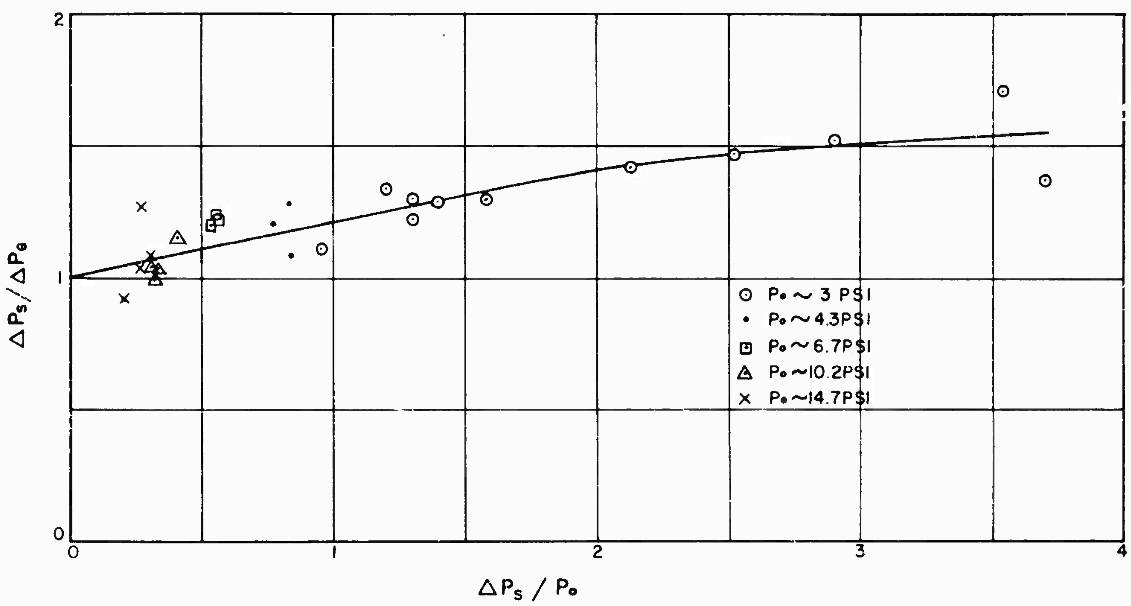

Figure B.3 Shock tube calibration of pressure probe. Axis of probe at 45° to shock normal.

were used on these measurements; however, the damping orifice size was varied, 0.075-, 0.109-, and 0.125-inch-diameter orifices being used at each ambient pressure. There is some indication of a slight decrease in $\Delta P_s / \Delta P_g$ with increase in the size of the damping orifice, but this can probably be attributed to a slight bias in the smoothing and extrapolation caused by the increase in overshoot on the first peak with decreased damping. Since the statistical significance of this apparent trend is dubious, these points are plotted in Figure B.3 without distinction as to orifice size.

For use in correcting the field data, it is convenient to replot the smoothed curves of Figures B.1, B.2, and B.3 with $\Delta P_g / P_o$ instead of $\Delta P_s/P_o$ as the independent variable, since ΔP_g is the quantity obtained directly from the recorded traces. This was done in Figure 2.1. In Shot 10, the angle θ between the axis of the pressure probe and the normal to the shock wave front varied from 72 degrees to 83 degrees over the canister array, and the correction factors used were obtained by interpolation between the 45-degree and 90-degree curves of Figure 2.1.

Appendix C

NOTES ON TELEMETERING PERFORMANCE ON SHOT 10

In all operations with the telemetering pressure canisters, it has been the practice to record the RF carrier signal strength along with the output of the sub-carrier information channels as a general check on the operation of the system. In all three shots of Operation Teapot on which the canisters were used, an abrupt drop in carrier signal strength was noted at zero time. The time in which this drop takes place is less than the response time of the galvanometers used, i.e., it is less than about 2 or 3 msec. The recovery time is much longer, of the order of a few tenths of a second, but accurate figures cannot be given, since the received signal strength depends on the orientation of the canister antenna and usually exhibits oscillations due to the swaying of the canister on its parachute suspension. It is not believed that this drop in carrier signal strength is caused by the electromagnetic transient that has sometimes caused loss of data in surface measurements due to the induction of strong signals in long transmission lines. This transient is of very short duration, and there appears to be nothing in the canister circuitry that could be responsible for the relatively slow recovery. It is suggested that ionization produced by gamma radiation is the most probable explanation, since the time scale of the recovery appears to be commensurate in order of magnitude with the rate of decay of prompt gamma radiation after its initial peak. The effect of intense gamma radiation on radio telemetry in the 200-to-230-Mc band was investigated by the AFSWP--Johns Hopkins University group that made measurements of shock velocity in the free air region on moored balloons during shots Dog and Easy of Operation Greenhouse (Reference 12).

Neither the Greenhouse nor the Teapot results permit a clear separation of the direct effect of gamma irradiation on transmitter output and the effect of attenuation over the propagation path due to ionization of the intervening atmosphere. In Reference 12 it is reported that no effect was noted when a complete transmitter was subjected to an estimated radiation flux of 10 r/sec under a 2-Mev X-ray machine. However, in Shot 10 all canisters with the exception of the most distant three, No. 13, 14, and 15, were subjected to peak-gamma-dosage rates considerably greater than 10^4 r/sec, so that the X-ray test is not particularly relevant. The total gamma dosage, estimated gamma dosage rate at 0.01 second, and the percentage drop in RF carrier signal strength at zero time are given in Table C. 1. The figures for total integrated dosage are those obtained by Project 2. 1 from film badges and chemical dosimeters mounted in the canisters (Reference 13). These are preliminary values, not corrected for canister motion during the time of dosage accumulation, or for a possible effect of neutrons on the gamma dosimeters, but will serve to indicate orders of magnitude. Measured values were not obtained at shorter ranges than canister 3 at 915-feet slant range, but the extrapolated values given for canisters 1 and 2 should not be greatly in

TABLE C. 1 GAMMA RADIATION RATE AND R.F. ATTENUATION NEAR ZERO TIME

Canister No.	Slant Range at Zero Time (ft.)	Total Gamma Dosage (roentgens)	Gamma Rate at .01 Sec. (r/sec)	Attenuation of rf Signal at Zero Time (percent)
1	640	*3.73×10^5	2.5×10^6	82 (100% at t = .07)
2	720	*2.95 "	2.0 "	84 (100% at t = .06)
4	945	1.73 "	1.2 "	100 (continues 100% to t = .06)
5	1180	1.08 "	7.3×10^5	88
6	1500	6.04×10^4	4.1 "	85
7	1640	4.8 "	3.3 "	81
8	2035	2.67 "	1.8 "	71
9	2600	1.40 "	9.5×10^4	58
10	3115	8.2×10^3	5.6 "	43
11	3720	4.8 "	3.3 "	31
13	7375	3.7×10^2	2.5×10^3	11
14	10000	93	6.2×10^2	5
15	12670	30	2.0 "	3.6

* = extrapolated values

error. The estimated gamma dosage rate was obtained by graphical differentiation of the curve of cumulative percentage of total dose versus time given in TM 23-200 (second edition). It will be noted that in order to simulate the radiation intensity to which canisters 1 through 4 were subjected it would be necessary to use a source capable of producing more than 10^6 r/sec. It is also a fact of some interest that radiation of the intensity received at canister No. 1 did not produce complete equipment failure, since at later times an intermittent signal was received from this canister. All of its parachutes were destroyed by blast or thermal radiation and it was in free fall and presumably tumbling when the signal returned. The intermittent, and roughly periodic, character of the return probably does not indicate intermittent transmission but merely that a signal

TABLE C.2 GAMMA RADIATION RATE AND R. F. ATTENUATION AT SHOCK ARRIVAL TIME

Canister No.	Shock Arrival Time (sec)	Slant Range at Shock Arrival (sec)	Gamma Rate (r/sec)	Attenuation of r. f. Signal (per cent) below Pre-Shot Value
1	*.096	638	4.5×10^5	88
2	*.124	710	2.9×10^5	100
4	.220	939	9.5×10^4	67
5	.359	1,126	4.1×10^4	45
6	.570	1,473	1.5×10^4	24
7	.630	1,566	1.2×10^4	Not measureable: attenuation less than variation in signal strength due to normal canister oscillation.
8	.941	1,964	4.1×10^3	
9	1.380	2,492	1.6×10^3	
10	1.810	2,988	6.5×10^2	
11	2.338	3,580	3.1×10^2	
13	5.495	6,944	10	
14	7.830	9,378	1.8	
15	10.244	11,849	0.4	

* = taken from NOL time-distance curve

was received only when the canister antenna passed through a favorable attitude with respect to the receiving station.

In Table C.2 the corresponding figures for gamma radiation rate and percentage RF signal attenuation are given for the time of shock arrival at each canister. Since data were successfully transmitted from canister No. 4, it appears that a radiation rate at the canister of more than 10^5 r/sec would be necessary to cause a serious loss of signal strength. Actually, although the geometry of the telemetering propagation paths at Shot 10 was not such as to provide definite proof, it is believed that the direct effect of gamma radiation on the transmitter is a relatively minor factor, and that most of the observed attenuation should be attributed to ionization of the atmosphere along the transmission path.